



**HAL**  
open science

## Clouds in current and in a warming climate

Caroline Muller

► **To cite this version:**

Caroline Muller. Clouds in current and in a warming climate. Fundamental Aspects of Turbulent Flows in Climate, Volume 108, August 2017, 2020. hal-03023276

**HAL Id: hal-03023276**

**<https://hal.science/hal-03023276v1>**

Submitted on 25 Nov 2020

**HAL** is a multi-disciplinary open access archive for the deposit and dissemination of scientific research documents, whether they are published or not. The documents may come from teaching and research institutions in France or abroad, or from public or private research centers.

L'archive ouverte pluridisciplinaire **HAL**, est destinée au dépôt et à la diffusion de documents scientifiques de niveau recherche, publiés ou non, émanant des établissements d'enseignement et de recherche français ou étrangers, des laboratoires publics ou privés.

# 1

## Clouds in current and in a warming climate

---

Caroline Muller

*CNRS, Laboratoire de Météorologie Dynamique, École Normale Supérieure Paris*

Lecturer picture from the summer school to be added

## 1.1 Introduction

We see them in our everyday lives. They make skies and sunsets even more beautiful, inspiring painters all over the world. But what are clouds? What are the physical processes occurring within a cloud? Do they all look alike, or are there different types of clouds? Why? Beyond our small human scale, how are clouds distributed at large, planetary scales? How do they couple and interact with the large-scale circulation of the atmosphere? What do the physics of cloud formation tell us about the hydrological cycle, including mean and extreme precipitation, in our current climate and in a warming world? What role do they play in the global energetics of the planet, for instance by reflecting the incoming shortwave radiation from the sun, and by reducing the outgoing longwave radiation to space, because of their high altitudes and thus cold temperatures? These are the questions that will be addressed in these five lectures.

The two first lectures will review well-understood aspects of cloud distribution and physics, which can also be found in various classical textbooks (which will be referred to at the relevant places). More specifically, the first lecture, *Cloud fundamentals*, will describe the fundamental properties of clouds: global distribution, cloud types, cloud visualization from satellites in space, and link with the large-scale circulation. The second lecture, *Cloud formation and physics*, will focus on the physics of clouds. We will briefly review the important results from atmospheric thermodynamics, and their implications for convective instability and cloud formation.

Then the last three lectures will address three key open questions about clouds in our current and in a warming climate. The third lecture, *Organization of deep convection at mesoscales*, addresses the issue of spatial organization of convection (here and in the following, convection refers to overturning of air within which clouds are embedded). The most spectacular example of organized convection is arguably the tropical cyclone, with its eye devoid of deep clouds, surrounded by the eyewall where winds among the strongest on the planet are found. Despite the extreme weather and thus the strong societal impact of organized convection, the physical processes at stake are not fully understood. Recent advances on this topic will be presented. Clouds are also tightly linked with precipitation and the fourth lecture, *Response of the hydrological cycle to climate change*, will review recent results on the response of the hydrological cycle to climate change, including both mean and extreme precipitation. The fifth and last lecture, *Clouds in a changing climate*, will review the effect of clouds on climate sensitivity (climate sensitivity refers to the temperature increase at equilibrium in response to a doubling of carbon dioxide concentrations), how this effect is quantified, as well as recent theoretical advances on the response of clouds to climate change including the so-called “fixed anvil temperature” or FAT hypothesis.

These last three topics are still very active areas of research, and for each we will review the state-of-the-art and present some recent advances made possible in recent years by the increased computational power as well as increased fundamental understanding of moist convection.

## 1.2 Cloud fundamentals

### 1.2.1 Spatial distribution of clouds : overview

What are clouds? The definition from the World Meteorological Organization of a cloud is a “hydrometeor consisting of minute particles of liquid water or ice, or of both, suspended in the atmosphere and usually not touching the ground. It may also include larger particles of liquid water or ice, as well as non-aqueous liquid or solid particles such as those present in fumes, smoke or dust.” In other words, clouds are suspensions of liquid and ice water in the atmosphere. Note that, although there is water vapor in clouds - in fact there is water vapor everywhere in the troposphere-, this is not what we see. Indeed our eyes are not sensitive to water vapor, instead what makes a cloud visible are the liquid and/or ice particles that it contains.

Looking at a daily weather map of deep clouds, see e.g. the website (EUMETSAT, 2017), confirms the diversity of cloud dynamics (see figure 1.1 for a snapshot). This map shows a one-year long evolution of weather and clouds derived from infrared satellite measurements, which are sensitive to cloud top temperatures, thus to high and deep clouds reaching cold high altitudes. The distribution of clouds is not uniform, and varies greatly with latitude.

The rich dynamics of deep clouds include small-scale, “pop-corn” like, deep convection in the tropics, notably convection associated with the diurnal cycle above tropical continents (e.g. central Africa close to the equator). In the tropics, corresponding to the rising branch of the Hadley circulation known as the inter-tropical convergence zone (ITCZ), deep clouds yield cold cloud-top temperatures. Deep clouds can span the whole depth of the troposphere, from the top of the planetary boundary layer, to the tropopause, around 15 km at tropical latitudes.

Also notable at mid latitudes (around  $\pm 45^\circ$  latitude) are large-scale cloud systems associated with extra-tropical cyclones and their associated frontal systems. Deep clouds are embedded in frontal low and high pressure systems typical of those latitudes. More precisely clouds and high water vapor concentrations can be found on the eastward side of cold fronts.

Smaller cloud areal coverage is found in the subtropics (centered around  $\pm 30^\circ$  latitude), i.e. in the subsiding branch of the Hadley circulation, as can also be seen in the time-mean spatial distribution of cloud amounts and cloud top temperatures figure 1.2. The data is from the ISCCP project, whose website provides useful information and data on clouds (ISCCP, 2009; Rossow and Schiffer, 1999). In the subtropics, warmer cloud-top temperatures are consistent with the occurrence of shallow clouds (typically one to two kilometers in height).

Globally, clouds cover a large fraction of our planet, about two thirds (figure 1.2). The zonal mean makes clear that high cloud coverage is found in the tropics (close to the equator, within  $10^\circ$  latitude or so) and at mid latitudes (centered around  $\pm 45^\circ$  latitude). The largest cloud cover is over the southern ocean, and more generally larger cloudiness is found over oceans than over land.

Clouds are thus key actors of the climate system, as they cover a significant fraction of the planet. Indeed, depending on their thickness and their height, clouds can interact with the Earth radiation budget in different ways. Clouds cool the planet by reflecting

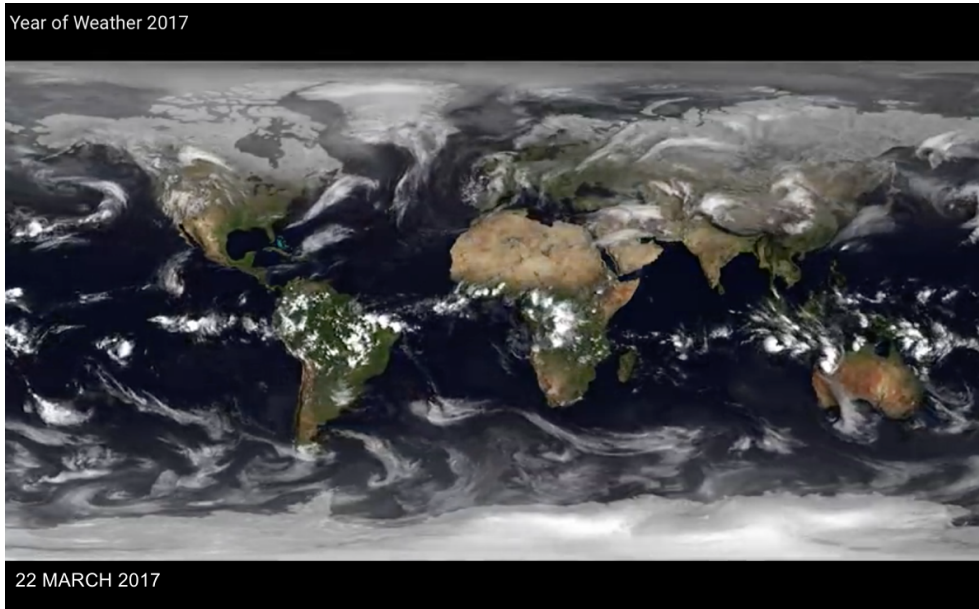


**Fig. 1.1** Snapshot from the 2017 “Year of Weather” online one-year long animation of high clouds from satellites. ©EUMETSAT 2017.

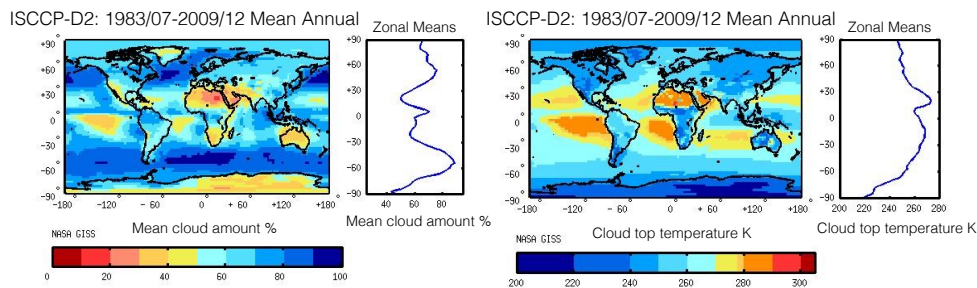


**Fig. 1.2** Time-averaged (1983 to 2009 estimated from ISCCP) distribution of cloud amount (fractional area covered by clouds, left) and cloud top temperatures (right) as a function of latitude and longitude. Also shown are zonal means as a function of latitude (blue curves). From ISCCP data (Rossow and Schiffer, 1999).

some of the incoming shortwave radiation from the sun. Clouds also warm the planet by trapping some of the longwave radiation emitted at the Earth surface, thus reducing the radiative cooling to space. Those radiative effects of clouds make them crucial ingredients of the global energetics. We will come back to this in the last lecture §1.6.

Consistently, understanding clouds, their coupling with a large-scale circulation, and how it impacts climate sensitivity, has been identified as one of the World Climate Research Programme (WCRP) grand challenge (Bony, Stevens, Frierson, Jakob,

Kageyama, Pincus, Shepherd, Sherwood, Siebesma, Sobel *et al.*, 2015). WCRP grand challenges represent areas of emphasis in scientific research in the coming decade, identifying specific barriers preventing progress in a critical area of climate science.

### 1.2.2 Cloud classification

Clouds are classified based on their appearance and altitude (Houze Jr, 2014). The classification is based on five latin roots:

- *Cumulus*: heap, pile;
- *Stratus*: flatten out, cover with a layer;
- *Cirrus*: lock of hair, tuft of horsehair;
- *Nimbus*: precipitating cloud;
- *Altum*: height.

Cumulus refers to clouds with some vertical extent, typically resembling “cotton balls”. Stratus refers to clouds with some horizontal extent, typically with a flat large horizontal cover. Cirrus characterizes the thin, filamentary aspect of the highest clouds almost entirely composed of ice crystals. Nimbus simply indicates precipitation reaching the ground, and altum is used to characterize mid-level clouds.

The roots are combined to define ten cloud types, shown on figure 1.3 and listed below from low to high (according to the height of cloud base):

- low clouds (cloud base below 2 km): cumulus, cumulonimbus, stratus, stratocumulus, nimbostratus;
- middle clouds (cloud base between 2 and 6 km): altocumulus, altostratus;
- high clouds (cloud base between 5 and 12 km): cirrus, cirrocumulus and cirrostratus.

Note that the cumulonimbus is classified as a low cloud because of its low cloud base. It may sound counter-intuitive to call it a low cloud given its significant vertical extent. Historically, clouds were classified according to cloud base because cloud observers were on the ground, making it difficult to estimate the cloud height. But now that modern observations are from satellites in space, it becomes more common to classify clouds based on their cloud top height. The cumulonimbus would thus be called a high cloud, or even better a deep cloud.

### 1.2.3 Visualization from space (IR, VIS, WV)

A powerful tool to investigate cloud properties and distribution is visualization from satellites in space. Clouds can be visualized in several channels, including the infrared channel, giving the emission temperature which helps detect high cold clouds; the visible channel, giving access to the albedo which helps detect low and high clouds thick enough to reflect sunlight; and the water vapor channel, which gives information on the flow and the water vapor advection (figure 1.4). Note that the VIS (visible) map has partial coverage, as information is not available at night. The interactive website of the University of Wisconsin-Madison (SSEC, 2018) allows the browsing of views from various geostationary satellites, and is a useful resource to become familiarized with these products.

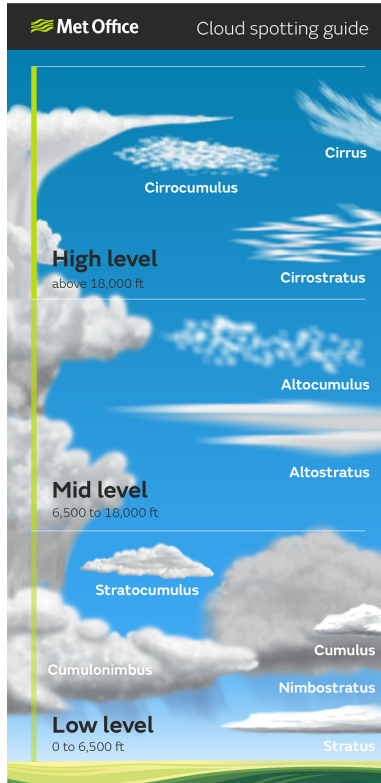


**Fig. 1.3** Cloud classification. Figure from the Met Office online cloud spotting guide <http://metoffice.gov.uk>. © British Crown copyright, Met Office.

#### 1.2.4 Link with the large-scale circulation

Clouds are tightly coupled to the large-scale circulation. Indeed, clouds form where there is upward motion, for reasons that will be discussed in §1.3 (briefly, colder temperatures at higher altitudes favor the condensation of water vapor into cloud liquid or cloud ice). In this section, we describe the distribution of clouds at planetary scales (thousands of kilometers), and its relation with the Hadley and Walker global cells, as well as Monsoon systems. Then we review the distribution of clouds at synoptic scales (hundreds to thousands of kilometers), and its interaction with equatorial waves and mid-latitude frontal systems.

We focus on tropical, subtropical and mid-latitude clouds which have specific sets of dynamics. In other words we will not discuss polar clouds. We note in passing that there is also organization of convection at mesoscales (a few hundred kilometers), taking the form of mesoscale convective systems (these include squall lines, mesoscale convective complexes, and tropical cyclones), whose link with the large-scale circulation is still not fully understood, and the subject of active research. We will come back to this in §1.4.

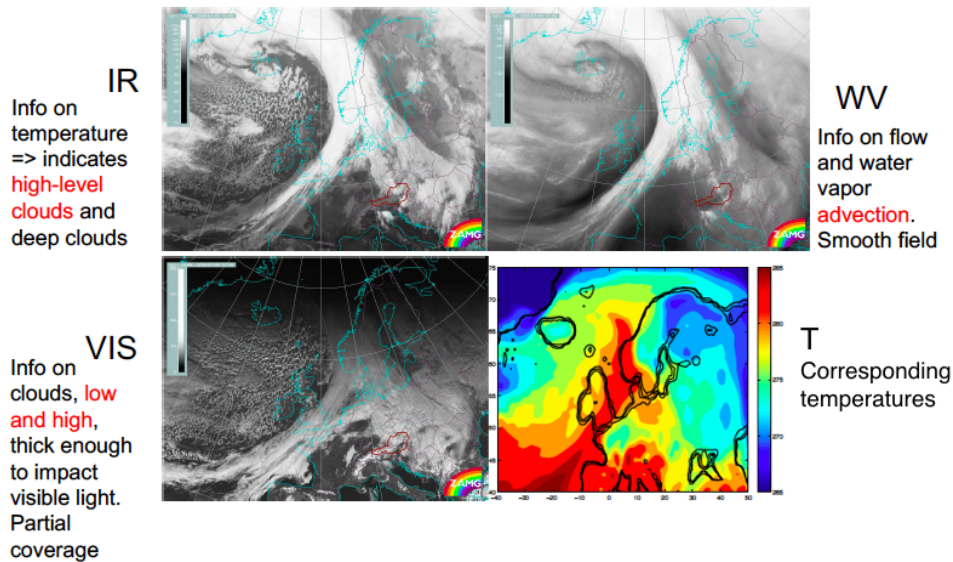


**Fig. 1.4** Cloud visualization from space in the infrared, water vapor and visible channels, from the Zentralanstalt für Meteorologie und Geodynamik (ZAMG) website (courtesy: Guillaume Lapeyre; data from ERA40 (Uppala et al., 2005 Quart. J. Roy. Meteor. Soc.)).

*Planetary scales.* Looking at sections of cloud fraction and circulation around the intertropical convergence zone (ITCZ) shows a clear correlation between cloud fraction and large-scale upward motion, with deep convection in the tropics, and shallow convection in the subtropics where there is large-scale descent (figure 1.5). Deep clouds (i.e. clouds spanning the whole depth of the troposphere, from the surface to the tropopause) are found in the ITCZ, which corresponds to the rising branch of the Hadley cell in the tropics. Conversely, in regions of large-scale descent such as the descending branch of the Hadley cell in the subtropics, deep convection is suppressed by the stability and dryness of the middle troposphere. Clouds are thus confined to the planetary boundary layer (from the surface to 2 km or so). Consistently, precipitation tends to be larger in the tropics and smaller in the subtropics. The cloud fraction and precipitation map varies seasonally, accompanying the meridional motion of the ITCZ around the equator (the location of the ITCZ is linked to the global energy balance including insolation differences and ocean heat transport).

Clouds are also embedded within the Walker cell, with deep convection occurring above the warm waters of the warm pool, corresponding to the rising branch of the Walker cell. Looking at the El-Niño Southern Oscillation (ENSO), which is the main mode of inter-annual variability of the Walker cell, we can see that the deep clouds move zonally, following the zonal shift of the upward motion. Both Asian and West African monsoons have signatures in cloud fraction and cloud content as well, similarly consistent with the location of upward motion.



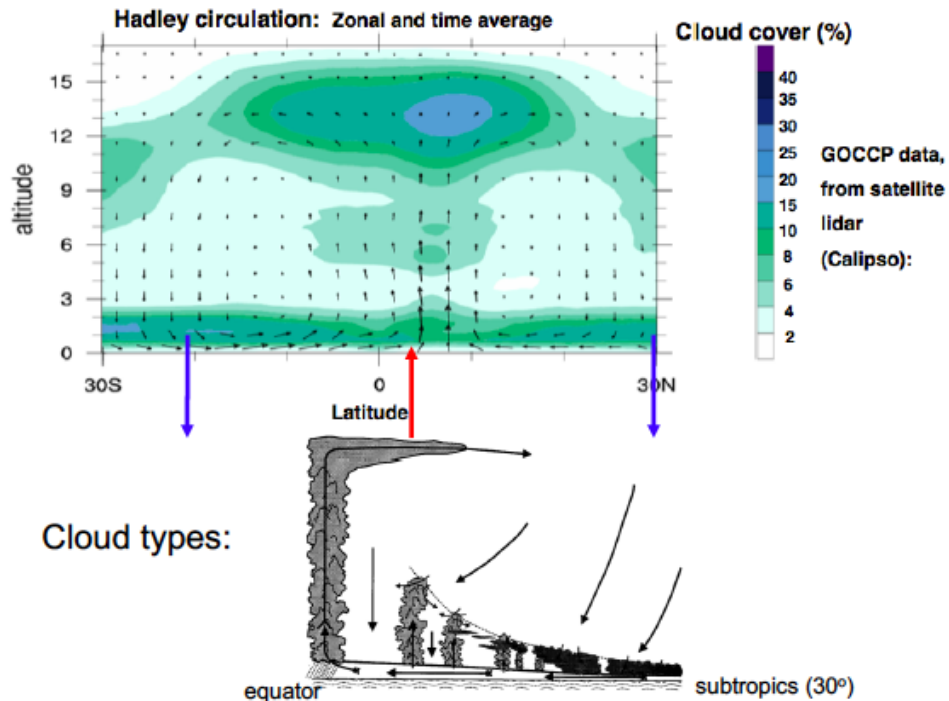


**Fig. 1.5** Top: Cloud fraction as a function of height and latitude, zonally and temporally averaged (green), along with the mean circulation (arrows) from the CALIPSO-GOCCP product (courtesy: Gilles Bellon). Bottom: Schematic of the latitudinal distribution of clouds, with deep clouds in the tropics and shallow clouds in the subtropics (adapted from Emanuel, 1994 Chapter 14); © 1994 Oxford University Press, Inc.

*Synoptic scales.* The synoptic scale has more subtle dynamics. In the tropics, the Coriolis parameter is small, and an important source of synoptic variability comes from equatorial waves. In the extratropics, the Coriolis force is dynamically important, and the leading order dynamics is quasi-geostrophic. This leads to the formation of synoptic frontal systems (fronts refer to regions with strong horizontal temperature gradients; see e.g. the strong temperature gradients found over Europe figure 1.4), within which clouds are embedded, as described in more details below.

- Equatorial waves

Let's start with the tropical atmosphere and see how equatorial waves lead to convective organization. Adopting the shallow-water formalism of Matsuno for the tropical atmosphere (Matsuno, 1966), we can write the inviscid shallow-water equations linearized around a state of rest. Assuming the Coriolis parameter,  $f$ , linearly proportional to distance from the equator (i.e.,  $f = \beta y$  a suitably valid approximation for motions in the tropics), the equations in usual notations are:

$$\frac{\partial u}{\partial t} - \beta y v = -g \frac{\partial \phi}{\partial x}, \quad (1.1)$$

$$\frac{\partial v}{\partial t} + \beta y u = -g \frac{\partial \phi}{\partial y}, \quad (1.2)$$

$$\frac{\partial \phi}{\partial t} + H \left( \frac{\partial u}{\partial x} + \frac{\partial v}{\partial y} \right) = 0, \quad (1.3)$$

where  $\phi$  denotes geopotential height, and  $H$  the depth of the undisturbed layer. Note that this system does not necessarily support plane wave solutions in  $(x, y, t)$  since one of the coefficients,  $\beta y$ , depends on the coordinate  $y$ . However this system yields wave solutions in  $(x, t)$  whose amplitude varies with  $y$ , i.e. solutions of the form  $\propto \hat{A}(y)e^{i(kx+\omega t)}$ . Specifically, one finds various types of trapped waves whose amplitudes decay in the  $y$ -direction.

The applicability of shallow water theory to equatorial convectively-coupled waves is by no means obvious. However the impressive match obtained by Wheeler and Kiladis (Wheeler and Kiladis, 1999) between observed equatorial variability (based on observed outgoing longwave radiation anomalies, see also (Kiladis, Wheeler, Haertel, Straub and Roundy, 2009) for a review) suggests that a portion of deep convection in the tropics is consistent with this theory. Agreement is also seen on Hovmoller diagrams of outgoing longwave radiation figure 1.6.

- Frontal systems and clouds

In the extratropics, cold and warm fronts are ubiquitous. Cold fronts refer to cold air masses advancing into warmer air. They tend to have sharp edges with high slope (figure 1.7) and deep convection. Warm fronts refer to warm air moving towards colder temperatures, and tend to have a shallower slope (figure 1.7). These fronts are for instance visible on figure 1.4, where sharp temperature gradients are clearly seen to be strongly correlated with cloud cover. Indeed, as cold air meets warm air, the warm air rises, thus giving rise to ascent and to cloud formation.

### 1.3 Cloud formation and physics

In the previous section, we saw that deep clouds are typically found in locations with large-scale upward motion, and suppressed in regions of large-scale subsidence. In this section, we discuss the physics of cloud formation, which will clarify this observation. The main references for this part are the two textbooks (Emanuel, 1994) and (Bohren and Albrecht, 2000).

#### 1.3.1 Atmospheric thermodynamics: dry convective instability

*The parcel method.* Cloud formation is closely related to the convective movement of air. Thus a key question is what makes the air move. Note that although temperature decreases with height, the cold air aloft is not heavier and thus does not “fall” to the ground, as its density is not only a function of temperature, but also of pressure  $\rho(T, p)$ . The three are related through the ideal gas law

$$p = \rho RT$$

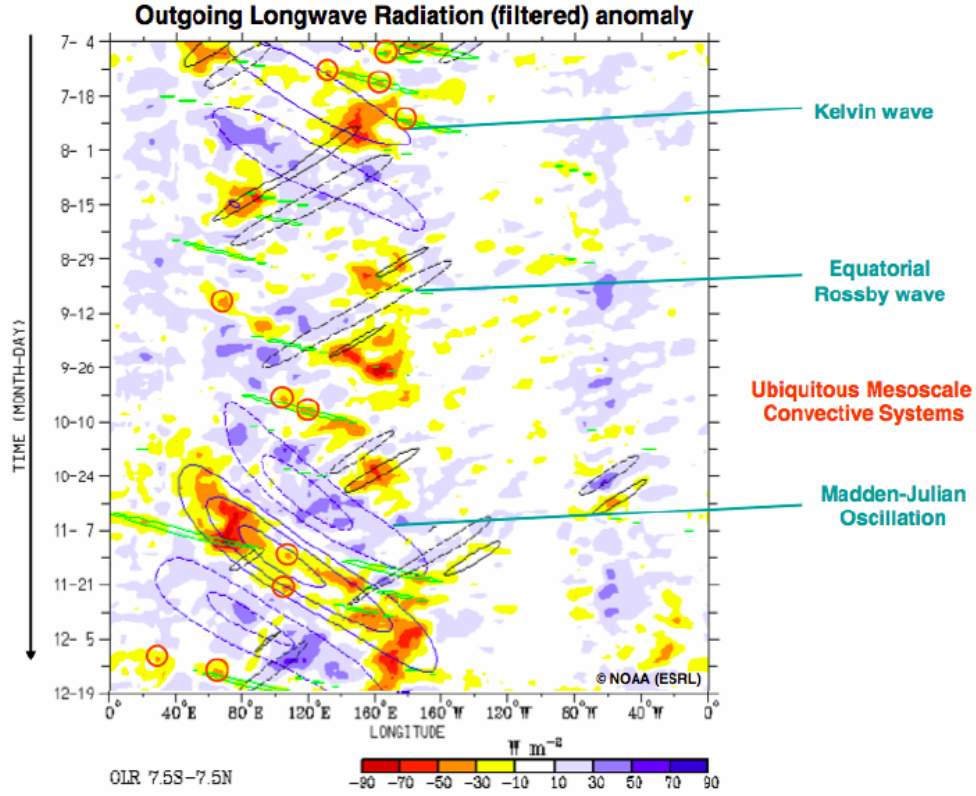


**Fig. 1.6** Time-longitude (Hovmöller) section of OLR anomaly averaged from 7.5S to 7.5N (time-mean and seasons removed, from ESRL-NOAA, courtesy: Gilles Bellon). Contours are anomalies filtered for the total OLR for specific regions of the wavenumber-frequency domain corresponding to the MJO (blue contours), Kelvin waves (green contours), and equatorial Rossby waves (black contours). Beyond the synoptic equatorial waves, we can also note the numerous smaller-scales (hundreds of kilometers) cloud clusters (red contours); these are mesoscale convective systems, and will be discussed in §1.4.

where  $R$  denotes the specific constant of the gas. This specific form of the ideal gas law is readily deduced from its molecular form  $pV = Nk_B T$ , where  $V$  denotes the volume of gas,  $N$  the number of molecules in  $V$ , and  $k_B$  the Boltzmann constant, by introducing the molecular mass  $m$ :  $p = (Nm/V)(k_B/m)T = \rho RT$  with

$$R \stackrel{\text{def}}{=} \frac{k_B}{m}. \quad (1.4)$$

Note that due to its dependence on the molecular mass of the gas, the specific constant depends on the gas considered.

To determine the stability of air, we thus need to account for changes in  $T$  and  $p$  with height. We use the so-called “parcel method” to assess whether a parcel of air is unstable to upward motion. We consider a hypothetical parcel of air near the surface

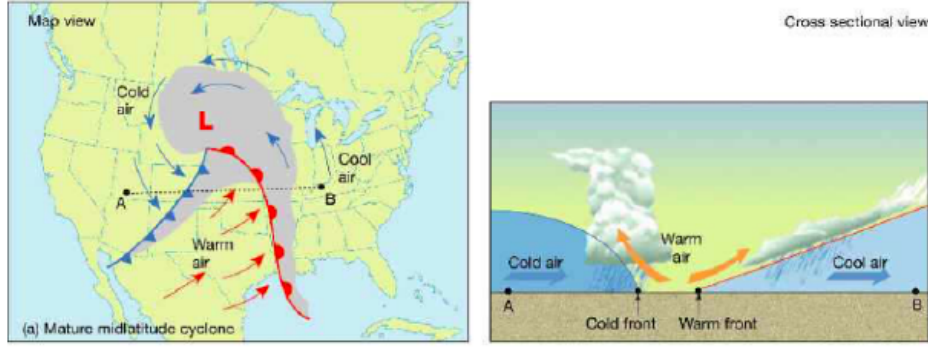


**Fig. 1.7** Top (left) and cross sectional (right) view of a cold front, schematized on weather maps as blue lines with triangles, and cold front, red line with half-circles. Clouds are embedded within these frontal systems, as the rising of warm air encountering colder heavier air, leads to cloud formation. From Lutgens et al., *The Atmosphere*, 2001, ©Pearson Education, Inc 2010. Reproduced by permission of the publisher.

displaced vertically adiabatically, and ask the following question: if this parcel of air is displaced upwards, will it return to its original position, or will it keep rising? If the displaced parcel has lower density than the environment, it is lighter and will keep rising: the atmosphere is unstable to dry convection. If instead its density is larger, it is heavier and will accelerate back down: the atmosphere is stable to dry convection. The displacement is supposed to be slow enough that the pressure of the parcel is always in equilibrium with the pressure of the environment (“quasi-static” displacement; see e.g. (Bohren and Albrecht, 2000) for a discussion of this assumption).

*Conservation of potential temperature.* We now show that during the quasi-static adiabatic parcel displacement, there is an invariant called *potential temperature*

$$\theta \stackrel{\text{def}}{=} T(p/p_0)^{-R/c_p}, \quad (1.5)$$

where  $T$  denotes temperature,  $p$  pressure,  $p_0$  a reference pressure (typically 1000 hPa), and  $c_p$  heat capacity at constant pressure. Then we will use this invariant to determine the condition under which the atmosphere is unstable to dry convection.

Applying the first law of thermodynamics to an infinitesimal displacement, the change in internal energy  $c_v dT$  is equal to the heat added, which is zero in this adiabatic displacement, plus the work done on the parcel, in that case due to pressure forces  $\delta W = -pd(1/\rho)$ :

$$c_v dT = -pd \left( \frac{1}{\rho} \right). \quad (1.6)$$

Using the ideal gas law  $p = \rho RT$  and recalling that  $c_v + R = c_p$ , we obtain

$$c_v dT = -p d \left( \frac{RT}{p} \right) = -RdT + RT \frac{dp}{p} \Leftrightarrow c_p dT + RT \frac{dp}{p} = 0 \quad (1.7)$$

## 12 short lecture title

implying

$$\frac{dT}{T} - \frac{R}{c_p} \frac{dp}{p} = d \ln(Tp^{-R/c_p}) = 0. \quad (1.8)$$

This shows that  $Tp^{-R/c_p}$  is constant, hence  $\theta = T(p/p_0)^{-R/c_p}$  is conserved during the displacement.

Before assessing the stability of the parcel, we note that in the special case of a hydrostatic atmosphere, i.e. assuming  $dp = -\rho g dz$ , the variable

$$h_{dry} \stackrel{\text{def}}{=} c_p T + gz \quad (1.9)$$

is conserved. It is called the *dry static energy*. Indeed if we make this hydrostatic approximation, equation (1.8) becomes

$$c_p dT + RT \rho g \frac{dz}{p} = d(c_p T + gz) = dh_{dry} = 0, \quad (1.10)$$

where we have again used the ideal gas law  $p = \rho RT$ . Thus the dry static energy  $c_p T + gz$  is conserved in an adiabatic quasi-static displacement under the hydrostatic approximation. Furthermore in that case, it is readily seen from equation (1.10) that the dry adiabatic lapse rate  $\Gamma_d$ , defined as the decrease of temperature with height, is given by

$$\Gamma_d \stackrel{\text{def}}{=} -\frac{dT}{dz} = -\frac{g}{c_p} \approx 10^\circ \text{ K / km}. \quad (1.11)$$

*How can we assess the stability of dry air?* We now return to the general case (relaxing the hydrostatic approximation) and to our original question, namely is the displaced parcel lighter or heavier than its environment. Recall that the pressure of the parcel is equal to that of the environment, so that during the displacement its pressure changes following the environmental pressure, while its temperature changes such that the potential temperature is conserved. To fix ideas, let's raise a parcel upwards (a similar argument can be made for downward displacements). Figure 1.8 schematically describes the three possible cases, depending on the environmental potential temperature profile  $\bar{\theta}$ , shown in red as a function of height.

The displaced parcel starts with the near-surface environmental value  $\theta_p = \bar{\theta}$ , and conserves its potential temperature  $\theta_p$  during its adiabatic ascent (blue). Once displaced, comparing  $\theta_p$  with  $\bar{\theta}$  at the displaced pressure level determines whether the parcel is heavier or lighter than the environment. If  $\bar{\theta}$  increases with height (left panel), the displaced parcel has colder potential temperature than the environment  $\theta_p < \bar{\theta}$ , and thus is heavier and accelerates back down: the atmosphere is stable to dry convection. On the other hand, if  $\bar{\theta}$  decreases with height (right panel), the displaced parcel has warmer potential temperature than the environment  $\theta_p > \bar{\theta}$ , and thus is lighter and keeps rising: the atmosphere is unstable to dry convection. If  $\bar{\theta}$  is constant with height (middle panel), the displaced parcel is neither accelerated downwards nor upwards: the atmosphere is neutral to dry convection.

In the stable case, the displaced parcel will accelerate back towards and passed its original equilibrium altitude. It will then be lighter than the environment and

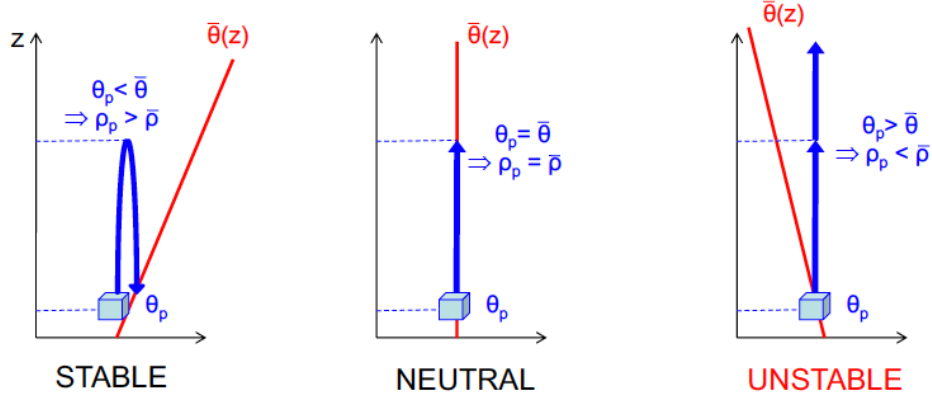


**Fig. 1.8** Schematic representation of the parcel method.

accelerate back up towards its equilibrium altitude. Thus the displaced parcel oscillates around its equilibrium height. The frequency of oscillation is known as the buoyancy frequency, or Brunt Väisälä frequency, and can easily be shown to be given by:

$$N = \sqrt{\frac{g}{\bar{\theta}} \frac{\partial \bar{\theta}}{\partial z}}.$$

In the unstable case, convection is very efficient at removing the instability. Indeed, in the planetary subcloud layer (first kilometer of the atmosphere or so), the convective adjustment time scale is very fast (minutes for dry convection) compared to destabilizing factors (surface warming, atmospheric radiative cooling...). Thus the observed state is very close to convective neutrality  $\bar{\theta} = \text{constant}$ , see for instance the review (Stevens, 2005) and references therein.

But above this thin boundary layer, this observation does not hold anymore and  $\bar{\theta}$  is observed to increase with height. This is because above the subcloud layer, atmospheric convection involves phase change of water vapor. We need to revisit the above calculations to account for the significant latent heat released during the phase changes of water. But let's first introduce the most common variables used to quantify the amount of water (vapor, liquid or ice) in the atmosphere.

### 1.3.2 Atmospheric thermodynamics: moist variables

Commonly used moist variables (Emanuel, 1994) are:

- Water vapor density (where  $M_v$  denotes the mass in kg of water vapor in the volume  $V$  in  $\text{m}^3$ ):

$$\rho_v \stackrel{\text{def}}{=} \frac{M_v}{V},$$

- Dry air density (where  $M_d$  denotes the mass in kg of dry air in the volume  $V$  in  $\text{m}^3$ ):

$$\rho_d \stackrel{\text{def}}{=} \frac{M_d}{V},$$

14 *short lecture title*

- Total air density:

$$\rho = \rho_v + \rho_d,$$

- Specific humidity:

$$q_v \stackrel{\text{def}}{=} \frac{\rho_v}{\rho},$$

- Mixing ratio:

$$r \stackrel{\text{def}}{=} \frac{\rho_v}{\rho_d},$$

- Partial pressure of water vapor  $e$ , satisfying the ideal gas law (where  $R_v$  denotes specific constant of water vapor, recall from equation (1.4) that its value depends on the gas considered; here  $R_v = k_B/m_v$  with  $m_v$  molecular mass of water):

$$e = \rho_v R_v T,$$

- Partial pressure of dry air  $p_d$ , satisfying the ideal gas law (where  $R_d = k_B/m_d$  denotes specific constant of dry air):

$$p_d = \rho_d R_d T,$$

- The total pressure is then given by Dalton's law:

$$p = p_d + e,$$

- Dew point temperature  $T_d$ : Temperature at which a parcel must be cooled at constant pressure to reach saturation (see next section for a discussion of saturation),
- Virtual temperature  $T_v$ : Temperature that dry air would have in order to have the same density as moist air at same pressure.

Let's derive the formula for the virtual temperature  $T_v$ , as a function of  $T$ ,  $r$  and the ratio of molecular mass of water vapor to dry air  $\epsilon$ :

$$\epsilon \stackrel{\text{def}}{=} \frac{m_v}{m_d} = \frac{R_d}{R_v} \approx 0.622.$$

By definition,  $T_v$  satisfies

$$p = \rho R_d T_v.$$

On the other hand, Dalton's law for partial pressures yields

$$p = \rho_v R_v T + \rho_d R_d T.$$

Therefore

$$T_v = T \left( \frac{\rho_v}{\rho_v + \rho_d} \frac{R_v}{R_d} + \frac{\rho_d}{\rho_v + \rho_d} \right) = T \left( \frac{1 + r/\epsilon}{1 + r} \right).$$

Note that since  $\epsilon < 1$ ,  $T_v > T$ , i.e. the virtual temperature is warmer than the actual temperature. This is expected since moist air is lighter than dry air, as the molecular mass of water vapor is smaller than the molecular mass of dry air. Therefore in order to have the same lighter density as moist air, dry air needs to be warmer.

### 1.3.3 Atmospheric thermodynamics: moist convective instability

What is the effect of moisture on convection? Beyond the virtual effect just discussed, i.e. water vapor making air lighter, an important impact of moisture on convection is the condensation and concomitant latent heat released (we will focus on vapor - liquid phase transition, though all the results below can be extended to the ice phase).

*When does water vapor condense into liquid water?* . The water vapor contained in air will condense when its partial pressure  $e$  exceeds a certain value, called the saturation partial pressure  $e_s$ . The latter is governed by the Clausius-Clapeyron equation, which can be derived using the thermodynamic equilibrium between liquid water and water vapor:

$$\frac{de_s}{dT} = \frac{L_v e_s}{R_v T^2}, \quad (1.12)$$

where  $e_s$  is the saturation vapor pressure,  $T$  the absolute temperature,  $L_v$  the latent heat of vaporization of water vapor and  $R_v$  the water vapor gas constant. There is net condensation when  $e > e_s(T)$ .

This law predicts that the saturation water vapor pressure strongly increases with temperature. A physical interpretation of this increase can be obtained by considering liquid water with a flat interface, above which water vapor is found with partial pressure  $e$ . Saturation corresponds to an equilibrium between evaporation from the liquid water below and condensation of the water vapor above.

- $e < e_s$  means that there is more evaporation than condensation,
- $e > e_s$  means that there is more condensation than evaporation,
- $e = e_s$  means there is as much condensation as there is evaporation.

Molecularly,  $e_s$  increases with temperature because the evaporation from the liquid phase increases with temperature, i.e. with the mean square velocity of the molecules. Thus the amount of water vapor required to equilibrate the evaporation is larger at larger temperatures.

We note here in passing that this is often phrased “warm air can hold more water vapor than cold air”. This is a useful shortcut to remember that the maximum amount of water vapor  $e_s$  attainable by a volume of air before it starts to condense, is an increasing function of temperature. But it gives the wrong impression that air is a “sponge” with holes in it, with the number of holes increasing with temperature. The saturation and condensation have nothing to do with “holes” in air, it simply has to do with equilibrium between evaporation and condensation. For a more in-depth discussion of the “sponge theory”, see e.g. (Bohren and Albrecht, 2000).

*Can we derive a conserved quantity for moist air?* We saw that to determine the stability of dry air, it was important to derive a conserved quantity under adiabatic displacements, namely the potential temperature  $\theta$  in equation (1.5). Can we derive a similar conserved quantity for moist air? The answer is yes, as we will now show, though this quantity, called equivalent potential temperature, is *approximately* conserved under adiabatic displacements.

For simplicity, we neglect the temperature dependence of the specific constant of air  $R$ , of the latent heat of vaporization  $L_v$ , and of the heat capacity at constant



pressure  $c_p$ , which in the following denote constants for dry air. We also neglect the virtual effect discussed above. For more details the reader is referred to (Emanuel, 1994).

As before, we apply the first law of thermodynamics to an infinitesimal displacement of a parcel of air. We first suppose that the parcel is saturated, i.e.  $q = q_s$  where  $q$  is the specific humidity and  $q_s$  the specific humidity at saturation. The only difference with our earlier dry case equation (1.7) is that we need to take into account the latent heat released during the condensation of water vapor  $-L_v dq$ , where  $dq$  denotes the change in water vapor specific humidity:

$$c_v dT = \delta W + \delta Q_{\text{cond}} = -p d\left(\frac{1}{\rho}\right) - L_v dq \quad (1.13)$$

$$\Leftrightarrow c_p dT - RT \frac{dp}{p} = -L_v dq \quad (1.14)$$

$$\Leftrightarrow d \ln \left( T p^{-R/c_p} \right) = -L_v \frac{dq}{c_p T} \approx d \left( \frac{L_v q}{c_p T} \right). \quad (1.15)$$

The latter approximation holds as long as

$$\frac{dq}{q} \gg \frac{dT}{T},$$

which is typically the case in the troposphere. We thus obtain

$$T p^{-R/c_p} \exp \left( \frac{L_v q}{c_p T} \right) = \text{constant},$$

leading to the introduction of a new variable approximately conserved for saturated adiabatic motion, the equivalent potential temperature:

$$\theta_e \stackrel{\text{def}}{=} \theta \exp \left( \frac{L_v q}{c_p T} \right),$$

where  $\theta$  is the dry potential temperature. Now note that in the case where the parcel is not saturated, there is no condensation of water vapor and  $q$  is conserved, so that  $\theta_e$  is also conserved. Thus  $\theta_e$  is (approximately) conserved under adiabatic motion, saturated or not.

Before investigating implications for the stability of air to moist convection, we first note that under the hydrostatic approximation, we can define the moist equivalent of the dry static energy in equation (1.9). It is called the moist static energy:

$$h \stackrel{\text{def}}{=} c_p T + gz + L_v q.$$

With the hydrostatic approximation,  $h$  is conserved under adiabatic displacements. Indeed from equation (1.14) and the ideal gas law,

$$dh = c_p dT + g dz + L_v dq \stackrel{\text{hydrostasy}}{=} c_p dT - \frac{dp}{\rho} + L_v dq \stackrel{(1.14)}{=} 0$$

How can we assess the stability of moist air?. Traditionally, skew-T diagrams are used in meteorology (figure 1.9), which allow to easily compare a measured temperature profile (red curve) to theoretical dry and moist adiabatic profiles (constant  $\theta$  and  $\theta_e$  respectively). Such diagrams have iso-temperature lines slanted at  $45^\circ$  to the right (slanted thin brown lines on the figure, hence the name “skew-T”; for more details on those diagrams, see the online MetEd module on Skew-T Mastery (COMET program, 2018)). Since temperature typically decreases with height, observed temperature profiles are largely vertical when reported on those diagrams. The green curve shows the observed dewpoint temperature, which is the temperature at which a parcel must be cooled at constant pressure to reach saturation. This dewpoint temperature curve depends on the environmental humidity (the more humid the air, the closer the dewpoint temperature is to the environmental temperature).

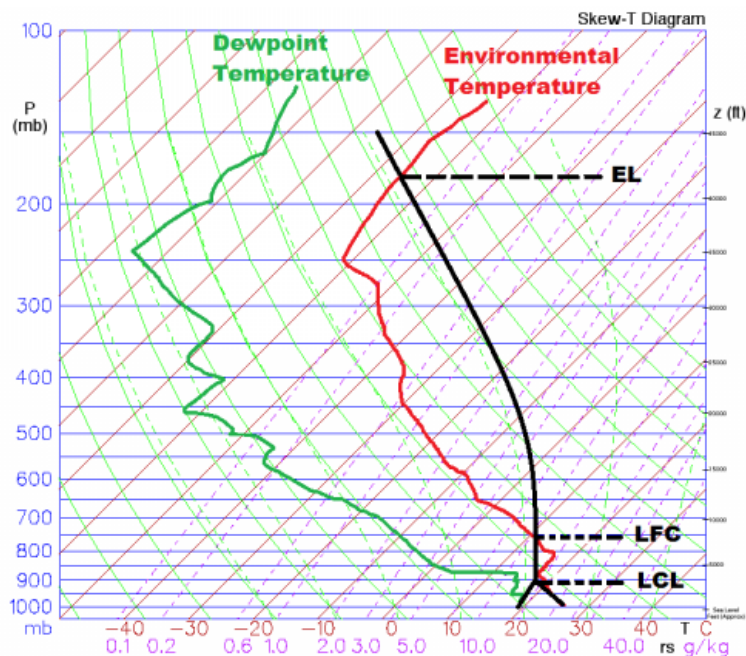


**Fig. 1.9** Skew-T diagram, showing observed temperature profile in red, observed dewpoint temperature in green. The parcel method consists of assessing the stability of a near-surface parcel to an upward displacement (parcel temperature shown in black). Adapted from the weathertogether.net blog.

We use the parcel method to evaluate the stability of this environmental temperature profile, by lifting a hypothetical parcel of air from the ground. Comparing, at a given pressure, the temperature of the parcel (shown in black) with the environmental temperature gives us information on its upward (warmer) or downward (colder) acceleration, and thus of its stability to vertical displacement.

- At first, the near-surface parcel is unsaturated. It thus follows a dry adiabatic

curve (line of constant  $\theta$ , thin green lines on the figure), until the lifted condensation level (LCL) is reached, where the parcel reaches saturation.

- Above the lifted condensation level,  $\theta_e$  will be conserved for the parcel which is undergoing moist adiabatic ascent (line of constant  $\theta_e$ , thin dashed green lines). Note that its temperature decreases with height slower than the dry adiabatic curve, due to the latent heat released as water vapor condenses.
- At a certain height, called level of free convection (LFC), the parcel becomes warmer than the environment. As long as this moist adiabatic curve is warmer than the environmental temperature profile, as “warm air rises”, the parcel is convectively unstable and keeps ascending.
- This ends when the parcel reaches its equilibrium level (EL), where the parcel’s temperature is equal to the environmental temperature.

In order to find the lifted condensation level, the dew point temperature is used, as well as lines of constant saturation mixing ratio iso- $r_s$  (thin dashed purple lines on the skew-T diagram). By definition of the dewpoint temperature, at the surface,  $r_s(T_{d,\text{sfc}}, p_{\text{sfc}}) = r_{\text{sfc}}$  where  $r_{\text{sfc}}$  is the water vapor mixing ratio of the parcel at the surface. The lifted condensation level is thus located where the iso- $r_s$  line passing through the surface dewpoint temperature intersects the parcel temperature.

*Convective Available Potential Energy (CAPE).* During the ascent, we just saw that the upward acceleration is related to the difference between the parcel temperature and the environmental temperature. This can be quantified further, in fact the area between the parcel and the environmental temperature is directly related to the potential energy of convection.

This can be clarified by considering the vertical momentum equation

$$\frac{\partial w}{\partial t} + u \frac{\partial w}{\partial x} + v \frac{\partial w}{\partial y} + w \frac{\partial w}{\partial z} = -g \frac{\rho'}{\rho} - \frac{1}{\rho} \frac{\partial p}{\partial z} + \nu \Delta w, \quad (1.16)$$

where  $\rho$  denotes the density of the environment,  $\rho'$  the density of the parcel minus that of the environment, and the last term is the viscous force. In strong vertical ascent, we can expect the leading order balance to be between the vertical advection and the buoyancy force

$$w \frac{\partial w}{\partial z} = -g \frac{\rho'}{\rho} \Leftrightarrow \frac{w^2(z)}{2} = \int_0^z -\frac{\rho'}{\rho} g dz. \quad (1.17)$$

The right-hand side has units of a specific energy. It represents an upper bound (as it neglects forces opposing the motion including viscosity and pressure gradients, as well as turbulent entrainment of less buoyant air at the edge of the rising plume) for the kinetic energy of the rising parcel. It is called the Convective Available Potential Energy, or CAPE.

CAPE can be rewritten as a function of temperature using the ideal gas law  $p = \rho RT$  and assuming that pressure perturbations between the parcel and the environment are small:

$$\frac{\rho'}{\rho} = -\frac{T'}{T}.$$

If we further make the hydrostatic approximation,

$$\text{CAPE} = \int_{p(z)}^{p(0)} \frac{T'}{T} \frac{dp}{\rho} = R \int_{p(z)}^{p(0)} T' d \ln p.$$

This expression shows that this convective potential energy is proportional to the area between the parcel and the environmental temperature on the skew-T ln  $p$  diagram shown in figure 1.9.

CAPE can be used to derive an upper bound for vertical velocities of buoyant parcels

$$w_{max} = 2\sqrt{\text{CAPE}}.$$

As mentioned earlier, for simplicity, we neglected virtual effects. We note though, that it is straightforward to include them in the above computation, yielding the more general formula

$$\text{CAPE} = R \int_{p(z)}^{p(0)} T'_v d \ln p.$$

Thus during the ascent, the area between the parcel temperature and the environment temperature on the skew-T diagram is a measure of atmospheric instability. The larger the CAPE, the stronger the upward motion during the ascent. If enough atmospheric instability is present, cumulus clouds are capable of producing severe convection and storms. In the following, we give a brief overview of the life cycle of such severe convective clouds. We also use the fundamental knowledge gained throughout this section to clarify the physical processes leading to cloud formation, for the different cloud types listed in §1.2.2.

#### 1.3.4 What are the processes leading to cloud formation?

We saw that condensation of water vapor, and thus cloud formation, occurs when the atmosphere becomes saturated. Saturation can occur through increased water vapor, but given the strong sensitivity of saturation water vapor pressure to temperature (governed by the Clausius-Clapeyron equation (1.12)), saturation very often occurs through cooling, for instance by the lifting of air to higher altitudes and thus colder temperatures, by contact with a cold surface or by radiative cooling.

*What are the leading physical mechanisms governing the formation and life cycle of deep convective clouds?.* In this section we describe the formation of deep clouds, i.e. cumulonimbus on figure 1.3 (and to some extent deep nimbostratus). Such clouds occur when the atmosphere is unstable, i.e. in the presence of CAPE.

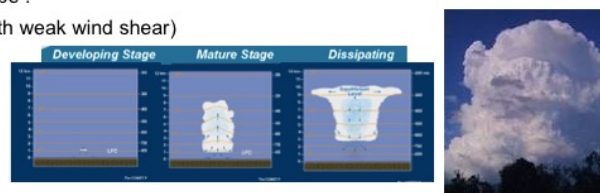
The formation of a typical single-cell storm (figure 1.10a) involves three stages (the interested reader is also referred to the MetEd module on Principles of Convection And Buoyancy (COMET program, 2018) for more details). The developing stage, as parcels ascend above the lifted condensation level, cool and saturate, thus forming a cloud. When the atmosphere is unstable (high CAPE), the ascent will continue during the mature stage to a high altitude until the equilibrium level is reached. Then in the dissipating stage, the cloud will spread horizontally at high levels and form an anvil cloud at high altitudes.

During this last stage, the falling precipitation partially evaporates at low levels, cooling the air, and forming downdrafts (descending pockets of cold air formed by

evaporative cooling). These downdrafts of cold, heavy air eventually hit the ground and spread horizontally as gravity currents. These are known as cold pools. Cold pools can help initiate other clouds by mechanically lifting moist air above the cold pool's boundary. Other lifting mechanism include orographic lifting (mechanical lifting above a mountain), or large-scale convergence and fronts (sharp temperature gradients). More generally, all forced ascent can lead to deep convection if the atmosphere above is unstable (i.e. high CAPE).

Note that thunderstorms can be :

(a) single-cell (typically with weak wind shear)



(b) multi-cell (composed of multiple cells, each being at a different stage in the life cycle of a thunderstorm).



(c) or supercell, characterized by the presence of a deep, rotating updraft

Typically occur in a significant vertically-sheared environment

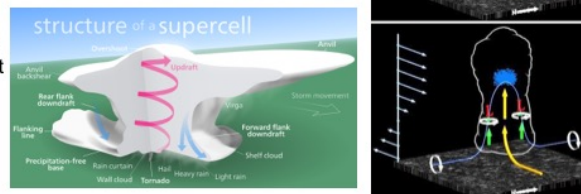


**Fig. 1.10** Life cycle of deep convective clouds. (a) single-cell, (b) multi-cell or (c) supercell storms. Adapted from the COMET<sup>®</sup> website at <http://meted.ucar.edu/> of the University Corporation for Atmospheric Research (UCAR), sponsored in part through cooperative agreement(s) with the National Oceanic and Atmospheric Administration (NOAA), U.S. Department of Commerce (DOC). ©1997-2017 University Corporation for Atmospheric Research.

The isolated single-cell cumulus cloud just described is the most common form of cumulonimbus. However, this single-cell storm can sometimes serve as the building block of a larger multi-cell storm (figure 1.10b), composed of multiple cells each being at a different stage in the life cycle of a thunderstorm. In the presence of strong vertical mean wind shear, supercells can form (figure 1.10c). These are characterized by the presence of a deep rotating updraft, and are associated with extreme weather, potentially causing significant damage. More generally, if enough atmospheric instability is present, i.e. in the presence of high CAPE, cumulus clouds are capable of producing severe storms.

*What are the leading physical mechanisms governing the formation of shallow clouds?* We now discuss the formation of clouds in shallow layers at low, middle and high levels (all but the cumulonimbus and nimbostratus on figure 1.3). Such clouds typically occur in a stable layer cooled from below, or in an unstable layer bounded above and below by a surface and/or a stable layer. For a more in-depth discussion of the dynamics of those different clouds, the interested reader is referred to (Houze Jr, 2014).

At low levels, we can distinguish two types of dynamics:

- Fog and stratus; these form in the planetary boundary layer when it is cooled from below, by radiation or/and conduction from a cold surface. In that case, the boundary layer is stable, and the air reaches saturation by cooling.
- Stratus or stratocumulus or shallow cumulus; these form in an unstable boundary layer heated from below, with a stable atmosphere above. The stable atmosphere aloft limits the convective motion to the bottom boundary layer. The radiative cooling at the top of the cloud layer can further destabilize the cloud layer and contribute to the convection.

In the latter case, there is an unstable layer capped by a stable layer. This is the case for instance when there is a so-called temperature inversion, i.e. when warm air is found above cold air. An inversion can develop aloft as the result of a frontal system advecting warm air above cold air, or in a high-pressure system with upper-level air gradually sinking over a wide area and being warmed by adiabatic compression. This is often the case in subtropical high-pressure systems associated with the descending branch of the Hadley cell. This explains why shallow clouds (e.g. stratocumulus, stratus) are very common in the subtropics (as we saw in e.g. figure 1.5). These shallow clouds at low levels can organize at the mesoscales, into open and closed cells. Not all is known about the organizational processes, but several mechanisms are believed to play a role, including background shear, thermal instability of the boundary layer, cloud-top entrainment and precipitation-driven cold pools.

At middle and high levels, shallow layer clouds also include:

- Cirriform clouds; these most often form by detrainment from deep convective clouds, consistent with the largest cirrus cloud cover in the tropics and in the extratropics where deep convection occurs. But they can also form away from generating sources, when an unstable layer is found aloft. These clouds are mainly composed of ice, and are found in an unstable layer between two stable layers. There is not much water vapor at those high altitudes, thus cirriform clouds are largely radiatively driven. The solar shortwave radiation heats throughout the cloud, while there is longwave cooling above and warming below the cloud layer.
- Altostratus and altocumulus clouds; these can be remnants of other clouds, in particular protruding layers at mid levels due to horizontal winds. Altocumulus are sometimes high-based convective clouds, with the same dynamics as deep convective clouds. Altostratus or shallow layers of altocumulus can also resemble a radiatively driven “mixed layer” aloft, leading to a cloud-filled layer radiatively cooled at its top.

## 1.4 Organization of deep convection at mesoscales in the tropics

In the previous section, we reviewed the physics behind the formation of individual clouds. But from §1.2, we know that clouds often organize at large scales, in particular at planetary and synoptic scales where they are tightly coupled to the large-scale circulation. It was also apparent from figure 1.6 that clouds often organize at mesoscales (hundreds of kilometers), into what are called mesoscale convective systems. The formation of such systems is still an active area of research, with important societal impacts, as it is associated with extreme weather and strong precipitation (see §1.5). It also has strong climatic impacts, as it affects the large-scale atmospheric radiation budget, by affecting cloud cover and the large-scale thermodynamic profiles (temperature and humidity, (Bony, Stevens, Frierson, Jakob, Kageyama, Pincus, Shepherd, Sherwood, Siebesma, Sobel *et al.*, 2015)). In this section, we focus on deep convective clouds in the tropics, and review the basics of mesoscale convective organization and the physical processes involved. We then discuss in more detail a recently discovered phenomenon in idealized simulations of the tropical atmosphere, namely the self-aggregation of convection.

### 1.4.1 Basics of convective organization

Organized convection refers to convection that is long-lived, i.e. that lasts longer than an individual convective cell (which typically lasts a few hours,  $< 3$  hours), and that grows upscale, i.e. that covers an area larger than an individual convective cell (which typically is  $< 10$  km across). The organization can arise from large-scale forcing, such as a sea-surface temperature gradient or the presence of land. It can also arise from the interaction with a large-scale flow, for instance the interaction of cold pools below precipitating clouds with a background vertical wind shear (see below). Or it can arise from internal feedbacks, leading to upscale growth in the absence of large-scale forcing, for instance self-organization of deep clouds by propagating waves or by “self-aggregation” feedbacks (see below).

Organized convection at mesoscales takes the form of mesoscale convective systems, or MCS. The American Meteorological Society (AMS) glossary defines an MCS as a “cloud system that occurs in connection with an ensemble of thunderstorms and produces a contiguous precipitation area on the order of 100 km or more in horizontal scale in at least one direction”. Mesoscale convective systems include squall lines, mesoscale convective complexes, or tropical cyclones (figure 1.11). Mesoscale convective complexes, or MCC, are a subset of MCS that exhibit a large, circular (eccentricity  $> 0.7$ ), long-lived ( $> 6$  hours), cold cloud shield. The cloud shield must have an area  $> 100\,000$  km<sup>2</sup> with infrared temperature colder than  $-32^{\circ}\text{C}$ , and an area  $> 50\,000$  km<sup>2</sup> with infrared temperature colder than  $-52^{\circ}\text{C}$ . Note that these are not mutually exclusive, in fact tropical cyclones can evolve from mesoscale convective complexes, and squall lines can be emitted from tropical cyclones and their outward spiraling bands of precipitation.

The leading physical processes for convective organization are an active area of research, with a lot of recent progress arising from the ability to simulate mesoscale systems, requiring large hundreds of kilometers domains, while resolving deep convection, requiring fine kilometeric resolution. These physical processes include:

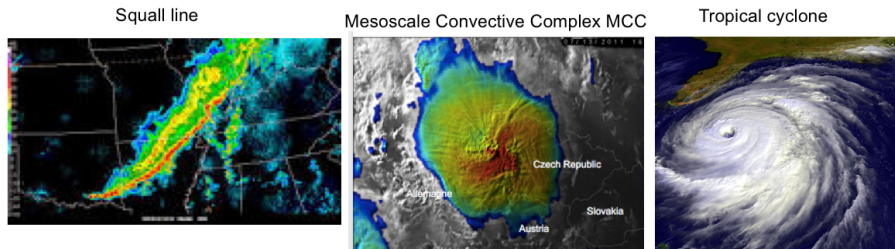


**Fig. 1.11** Mesoscale convective systems (MCS) include squall lines (radar image), mesoscale convective complexes or MCCs (from EUMETSAT Meteosat-8 satellite), or tropical cyclones (from NOAA GOES satellite).

- Vertical shear;
- Waves;
- Wind-induced surface heat exchange feedbacks;
- Convective self-aggregation feedbacks.

We describe each process in more detail below.

#### 1.4.2 Vertical shear

The presence of background vertical wind shear is known to favor the formation of squall lines. More precisely, the interaction of the shear with cold pools below precipitating clouds, is believed to be key in the formation of squall lines.

One possible explanation (figure 1.12a) is the advection of cold pools away from the convective updraft. Recall from the life cycle of convective clouds in §1.3.4 (see also figure 1.10a) that in the dissipating stage, the partial evaporation of the falling rain cools the air, creating cold heavy downdrafts, which hit the surface and spread horizontally. These pockets of cold air below clouds are known as cold pools, and inhibit further convection. In the case where the region with downdrafts and cold pools is advected away from the updrafts, as represented schematically in figure 1.12a, the updraft can persist on the upwind side of the cold pool, leading to long-lived convective clouds (Garner and Thorpe, 1992).

Another possible explanation is the interaction of the vorticity of the background shear with the vorticity of the spreading cold pool, which favors the formation of new updrafts and convective cells upshear (figure 1.12b). Note that in the previous theoretical explanation, the squall line is a system of long-lived convective cells, while in this case the squall line is a long-lived system of ordinary cells. (Rotunno, Klemp and Weisman, 1988) argue that the latter is more consistent with observations, though squall lines can occasionally be composed of long-lived supercell thunderstorms.

Consistently, in cloud-resolving simulations (right panels of figure 1.12), imposing a vertical wind shear, at low levels where cold pools are, yields the organization of clouds into arcs. The top panel shows a simulation without shear, in which the convection is somewhat randomly distributed, resembling “pop-corn” convection. The middle panel shows a simulation with critical shear, defined as the shear yielding squall lines perpendicular to the mean wind (in the  $x$  direction in these simulations from left to



right). This critical shear was empirically determined in these simulations, decreasing from  $10 \text{ m s}^{-1}$  at the surface to zero at 1 km. The last panel shows a simulation with supercritical shear ( $20 \text{ m s}^{-1}$  at the surface), in which the squall line orients itself at an angle with the background wind, so that the projection of the shear on the squall line is critical (Muller, 2013).

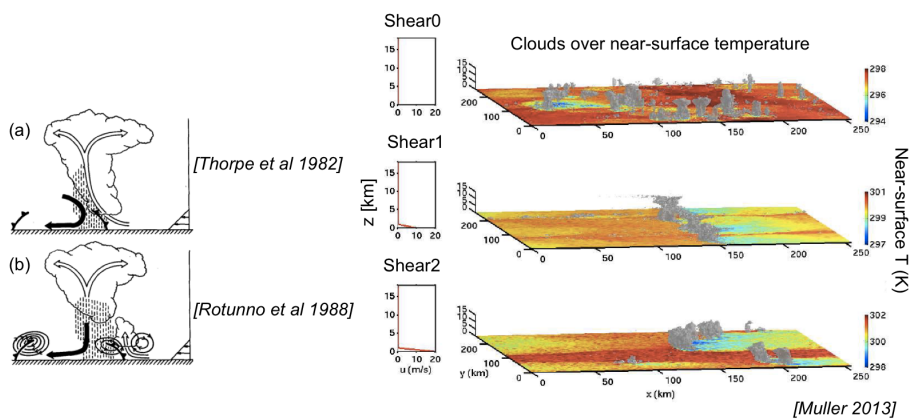


**Fig. 1.12** Left: Schematic interaction of a vertical wind shear with cold pools below precipitating clouds, adapted from (Rotunno, Klemp and Weisman, 1988); © 1988 American Meteorological Society (AMS). Right: 3D view of cloud-resolving simulations with different wind shear, in which convection organizes into arcs, adapted from (Muller, 2013); © 2013 American Meteorological Society (AMS).

### 1.4.3 Waves

Unlike in mid-latitudes, shear is often weak in the tropics. Thus shear alone can not explain all organized convective systems in the tropics. Additionally, in the tropics, upscale growth is ubiquitous and sometimes rapid, occurring beyond the extent of cold pools, and convective inhibition is small so that small perturbations can easily initiate new convection. Internal feedbacks, independently of a large-scale forcing or a large-scale circulation, are natural candidates to explain the observed organization of tropical clouds.

(Mapes, 1993) proposed that gravity waves, generated by the convection and propagating horizontally away from the convection (located at  $x = 0$  on figure 1.13), can destabilize the near-cloud environment and promote new convection nearby. Indeed, the deepest wave which warms and thus stabilizes the atmosphere, propagates the fastest. It is associated with subsidence throughout the troposphere (figure 1.13  $l = 1$  bore). The second mode ( $l = 2$  bore on the figure) is a baroclinic mode which propagates slower, and with cooling (through adiabatic ascent) at low levels. This lifting in the lower troposphere encourages convection close to the original cloud, allowing for convection to be “gregarious” (Mapes, 1993).

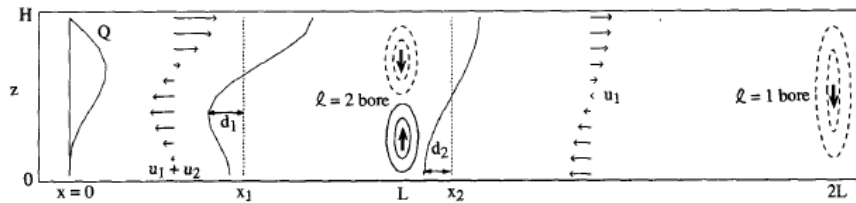


**Fig. 1.13** Schematic response to the heating associated with convection and clouds occurring at  $x = 0$ . The heating profile  $Q(z)$  is the sum of a deep mode with heating at all heights and a maximum at mid level, and of a baroclinic mode with cooling at low levels and heating at upper levels (Mapes, 1993). This distribution of heat excites waves that then propagate away from the convection, yielding adiabatic subsidence warming ( $l = 1$  bore and  $l = 2$  bore at upper levels) and adiabatic cooling through ascent ( $l = 2$  bore at lower levels); © 1993 American Meteorological Society (AMS).

#### 1.4.4 Wind-induced surface heat exchange (WISHE)

The so-called “wind-induced surface heat exchange”, or WISHE (Emanuel, 1986), is a positive feedback of convection on itself, related to enhanced surface fluxes in the moist convecting region. This feedback is particularly crucial for tropical cyclones, whose extremely strong surface winds in the eyewall yield enhanced surface fluxes there (mainly in the form of evaporation from the ocean). Thus the eyewall, which is the most energetic region where moisture and clouds are found, is the place where the surface fluxes of energy are strongest. In other words, surface fluxes enhance energy in the high-energy region, thus reinforcing energy gradients and yielding a positive feedback on the convective organization.

#### 1.4.5 Convective self-aggregation

An active area of research is linked to the spontaneous self-aggregation of convection. Self-aggregation refers to the spectacular ability of deep clouds to spontaneously cluster in space (see figure 1.14) despite spatially homogeneous conditions and no large-scale forcing, in high-resolution cloud-resolving models (CRMs) of the tropical atmosphere. These are models with fine, kilometer-scale resolution, i.e. simulations with sufficiently high spatial resolution to explicitly resolve the deep convection and deep clouds, instead of parameterizing them. Since its discovery in CRMs, the rapidly growing body of literature on self-aggregation confirmed its occurrence in a hierarchy of models, from two- and three-dimensional CRMs, to regional models and global climate models with parameterized convection, with super-parameterizations or without convective parameterization (Wing, Emanuel, Holloway and Muller, 2017).

This phenomenon was first discovered in idealized settings, namely non-rotating (Coriolis parameter  $f = 0$ ) radiative-convective equilibrium (RCE). This equilibrium is introduced next, followed by a more detailed discussion of the physical processes responsible for the self-aggregation of convection in non-rotating RCE simulations.

*Radiative-convective equilibrium.* Non-rotating RCE is an idealization of the tropical atmosphere, in which the rotation of the earth is neglected (a reasonable approximation

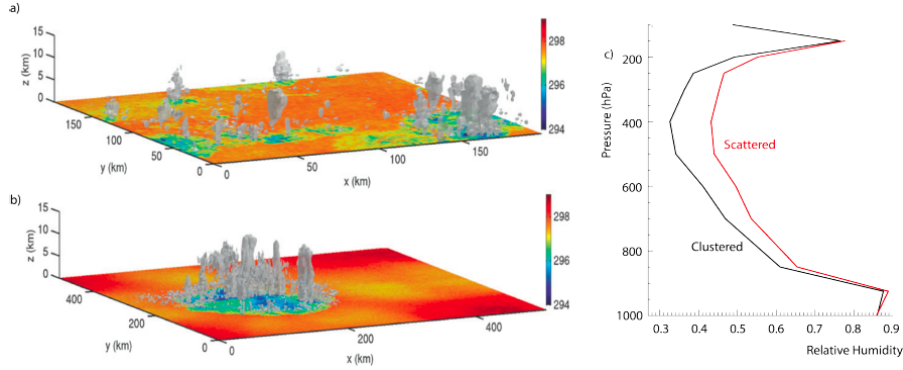


**Fig. 1.14** In models, convective organization (panel b) emerges spontaneously, increasingly so with increasing temperatures. It is associated with a large-scale drying of the atmosphere and enhance large-scale outgoing radiative cooling to space. In observations (panel c, relative humidity profiles from AIRS satellite measurements) the middle troposphere is drier in an atmosphere in which the same amount of precipitation is concentrated in a smaller number of convective clusters (adapted from Bony et al., 2015), consistent with modeled aggregation; © 2015, Springer Nature.

in the tropics where the Coriolis parameter  $f$  is small), and in which the large-scale motion (larger than the domain) is neglected. Thus there is no import or export of moist-static energy into or out of the domain, and the net atmospheric radiative cooling (top of atmosphere minus surface) must balance the input of energy into the atmosphere at the surface, namely latent and sensible heat fluxes. Over oceans, surface fluxes are largely dominated by the latent heat flux, so that in RCE over oceans, the net atmospheric radiative cooling is approximately equal to surface evaporation. From water conservation, the latter is equal to precipitation. In other words in RCE, the net atmospheric radiative cooling is in balance with the latent heating associated with the condensation of water vapor into precipitation by convection.

RCE is most easily understood by first looking at radiative equilibrium. Radiative equilibrium is the equilibrium state of the atmosphere and surface in the absence of non-radiative fluxes. In that case, radiative cooling and heating drive the atmosphere towards a state of radiative equilibrium. At radiative equilibrium, the incoming short-wave solar heating  $\pi R^2 S_0 (1 - a)$ , where  $R$  denotes the Earth radius,  $S_0$  incoming solar flux, and  $a$  albedo, exactly balances the outgoing longwave radiation  $4\pi R^2 \sigma T_e^4$  where  $\sigma$  is the Stefan-Boltzman constant and  $T_e$  the emission temperature (temperature with which a planet needs to emit in order to achieve energy balance), yielding:

$$\sigma T_e^4 = S_0 \frac{1 - a}{4}. \quad (1.18)$$

In the absence of atmosphere (left panel figure 1.15), the surface energy balance implies

$$\sigma T_e^4 = \sigma T_s^4 = S_0 \frac{1 - a}{4} \Rightarrow T_s = T_e = 255 \text{ K} = -18^\circ \text{ C},$$

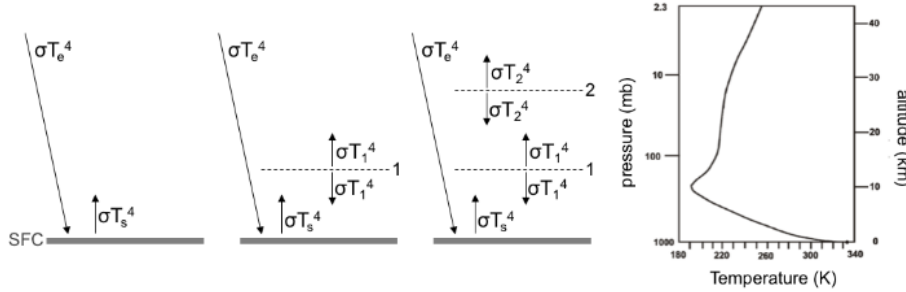


**Fig. 1.15** Radiative equilibrium without, with one or with two atmospheric levels (three left panels). The last panel shows the full calculation of radiative equilibrium (after Manabe and Strickler, 1964); © 1964 American Meteorological Society (AMS).

which is much colder than the observed mean surface temperature  $\approx 288 \text{ K} = 15^\circ \text{ C}$ . This warmer surface temperature is due to the presence of the atmosphere, and can be understood by adding a level to our simple conceptual model figure 1.15. We assume that the atmosphere is transparent to solar radiation, opaque to infrared radiation, and we assume black-body emission from the surface and each level (though the computation can easily be extended to account for emissivities smaller than 1). Energy balance at the surface and level 1 imply

$$\text{Level 1: } 2\sigma T_1^4 = \sigma T_s^4 \quad (1.19)$$

$$\text{SFC: } \sigma T_s^4 = \sigma T_e^4 + \sigma T_1^4, \quad (1.20)$$

yielding  $T_s = 2^{1/4} T_e = 303 \text{ K}$ , warmer than before.

If we add an additional atmospheric level (figure 1.15),

$$\text{Level 2: } 2\sigma T_2^4 = \sigma T_1^4 \quad (1.21)$$

$$\text{Level 1: } 2\sigma T_1^4 = \sigma T_s^4 + \sigma T_2^4 \quad (1.22)$$

$$\text{SFC: } \sigma T_s^4 = \sigma T_e^4 + \sigma T_1^4, \quad (1.23)$$

yielding  $T_s = 3^{1/4} T_e$ , even warmer.

The full calculation of radiative equilibrium was done by (Manabe and Strickler, 1964) and yields the temperature profile shown on the right panel of figure 1.15. Compared with observations, this profile is too hot near the surface, too cold near the tropopause, yielding a lapse rate of temperature which is too large in the troposphere (but the stratosphere temperature is close to the observed). In other words, the radiative equilibrium profile is unstable to moist convection.

The observed temperature profile in the troposphere is closer to a radiative-convective equilibrium profile. Physically, what happens is that radiation destabilizes the atmosphere by cooling the interior of the troposphere, thus making the lapse rate steeper. But the radiation time scale  $\approx 40$  days is much slower than the convective adjustment time scale  $\approx$  minutes for dry and hours for moist convection. Thus in the competition between radiation and convection, convection “wins”, and the observed state is much closer to convective neutrality than to radiative equilibrium. Convection has a stabilizing effect by bringing moist and hot air from the surface to the free-troposphere

(updrafts) and by bringing cold and dry air from the interior to the surface (down-drafts), thus reducing the lapse rate towards convective neutrality. More precisely, the vertical temperature profile is close to neutral to dry convection below the condensation level (dry adiabat  $\theta = \text{constant}$ ), and close to neutral to moist convection above (moist adiabat  $\theta_e = \text{constant}$ , see §1.3.3). It is this equilibrium between radiative cooling and convective heating which is referred to as RCE.

*Physical mechanisms of self-aggregation.* In simulations of RCE, illustrated in figure 1.14a, convection is somewhat randomly distributed, resembling “pop-corn” convection. Self-aggregation (figure 1.14b) can be seen as an instability of radiative-convective equilibrium, in which random pop-corn convection is replaced by a highly organized climate. Convection is confined to a subregion of the domain, and is surrounded by extremely dry air. In this section, we investigate in more detail the physical processes involved.

Most of the simulations described here are performed with the cloud-resolving model System for Atmospheric Modeling, or SAM (Khairoutdinov and Randall, 2003). Briefly, this model solves the anelastic momentum, continuity and scalar conservation equations. It is run here with fixed sea-surface temperature (close to current tropical values, 300 K), on a square domain with doubly periodic geometry. The horizontal resolution is on the order of one or a few kilometers, in order to resolve deep cloud processes. The domain size is a few hundreds of kilometers to allow mesoscale organization of convection. The vertical resolution is finer, tens of meters in the low troposphere increasing to 500 m in the mid-troposphere. A sponge layer is added in the upper third of the domain (18 km to 27 km altitude) in order to absorb gravity waves which would otherwise unrealistically fill the domain (see (Muller and Held, 2012) for more details).

From sensitivity experiments, i.e. simulations where the various feedbacks are turned on and off (e.g. surface flux feedbacks, radiative feedbacks...), we now know that longwave radiative feedbacks are crucial for self-aggregation (figure 1.16), at least at current tropical temperatures (Muller and Held, 2012). More precisely, the long-wave radiative cooling from low clouds in dry regions is found to be necessary for the spontaneous onset of self-aggregation from homogeneous initial conditions. When simulations are initiated from aggregated conditions though, the clear-sky radiative feedback from dry regions and the high-cloud radiative feedback from moist regions are also found to be sufficient to maintain the aggregation.

The importance of longwave radiative feedbacks for convective aggregation can be understood by considering the moist static energy transport between the dry and the moist regions. Note that in the tropics, horizontal temperature gradients are small, so that the variability in moist static energy is largely dominated by the variability of water vapor. Thus high energy regions correspond to moist regions and vice versa.

Figure 1.17 shows the circulation (black streamfunctions) in height and moisture space (Bretherton, Blossey and Khairoutdinov, 2005; Muller and Bony, 2015). The top panels show the circulation along with radiative cooling rates (left) and moist static energy (right). The arrows show the direction of the circulation. The strong radiative cooling in dry regions at low levels, which is largely due to the presence of low clouds (pink contours), generates subsidence (blue arrow) in the lowest kilometers of the dry

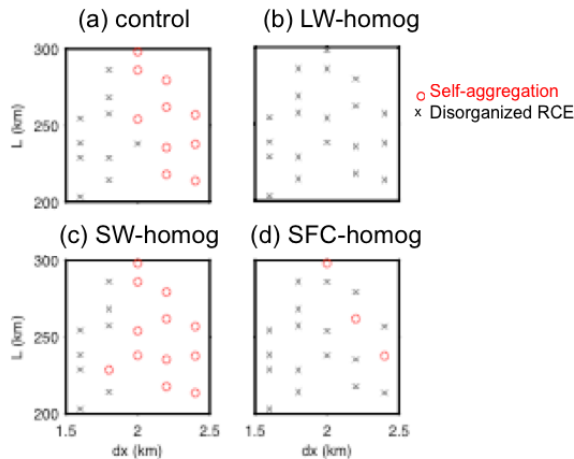


**Fig. 1.16** Results from sensitivity numerical simulations started from homogeneous initial conditions, in which various feedbacks are turned on and off. Simulations are shown as a function of domain size and resolution, and simulations that self-aggregate are shown as red circles. Although shortwave radiation feedbacks and surface flux feedbacks impact the range of parameters for which self-aggregation occurs, it is the longwave feedback which is found to be crucial for self-aggregation. Indeed, there is no spontaneous self-aggregation of convection when longwave radiative feedbacks are removed (after Muller and Held, 2012); © 2012 American Meteorological Society (AMS).

columns. This forces a near-surface flow (black arrow) from dry to moist columns. The high moist static energy near the surface is thus exported from the dry regions into the moist regions, yielding an upgradient energy transport. This is the positive feedback believed to be responsible for the strengthening energy gradients and concomitant self-aggregation of convection.

As mentioned above, even without the longwave radiative feedbacks from low clouds, convective aggregation can be maintained from aggregated initial conditions. The bottom panels show the same circulation, but in a simulation without low cloud longwave radiative contributions. The clear-sky low-level cooling in dry regions along with radiative warming from high clouds in the moist columns again yield subsidence in dry (blue arrow) and upward motion (red arrow) in moist regions. The near-surface flow associated with this dynamical response to the radiative cooling distribution (black arrow) again exports energy from dry regions to moist regions, yielding an upgradient energy transport.

In all cases, it is the low-level circulation, forced by differential radiative cooling rates between dry and moist regions, which is responsible for the upgradient energy transport yielding convective aggregation. Note that moist static energy is a strong function of height, thus the altitude of the radiative cooling and heating is important. In fact, (Muller and Bony, 2015) show that imposing enhanced radiative cooling in dry regions in radiative-convective equilibrium simulations can lead to the self-aggregation of convection, if the cooling is applied at low altitudes.

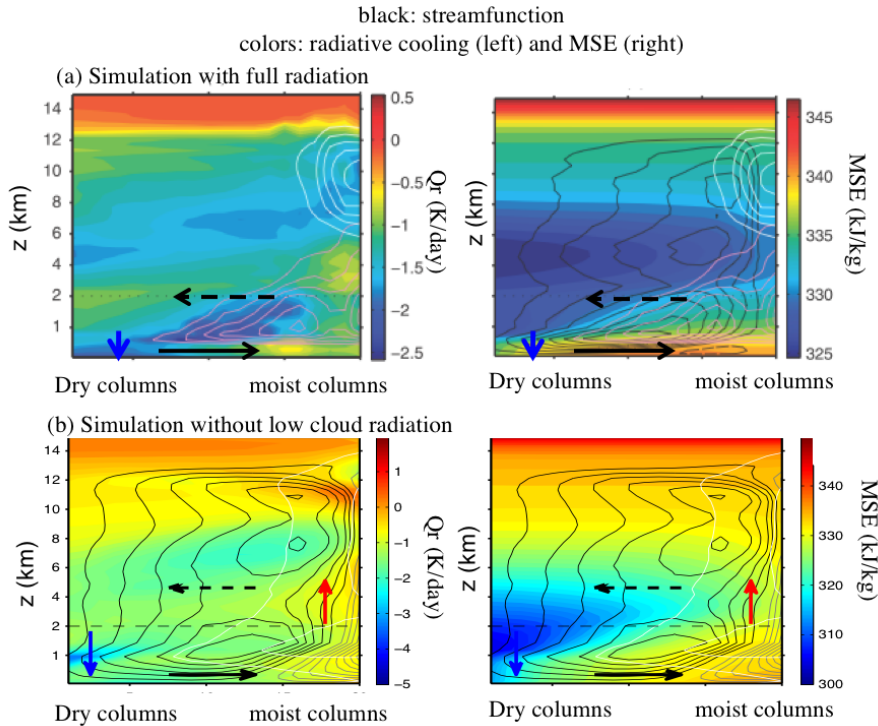


**Fig. 1.17** Circulation in height and moisture space (black streamfunction) in simulations that aggregate. The top panels show a simulation with full radiation, while the bottom panels show a simulation where the low-cloud longwave radiative feedback is removed (after Muller and Bony, 2015); © 2015, John Wiley and Sons.

A recent study has also been able to simulate self-aggregation even while suppressing radiation and other diabatic feedbacks (Muller and Bony, 2015) a result later confirmed in other models. The process leading to self-aggregation seen in these simulations has been called "moisture-memory" feedback, since it relies only on intrinsic interactions between clouds and the water vapor around them to spontaneously organize into clusters. It occurs when the evaporation of the falling rain is suppressed (i.e. at unrealistically high precipitation efficiency). The physical process leading to aggregation in that case is still unclear, but the absence of downdrafts below deep clouds when the evaporation of rain is suppressed is hypothesized to be important.

In standard conditions, the cooling associated with the evaporation of rain below deep convecting clouds generates downdrafts, which through their thermodynamical effect oppose the upward motion that generated the cloud. This negative feedback on upward convection suppresses the deep cloud in a few hours. Without the evaporation of rain and the effect of the associated downdrafts, moist areas remain moist (or even get moister by convergence) and thus become even more favorable to convection. This tends to localize the convection, as observed in these simulations.

This spontaneous self-aggregation of deep convection could have numerous implications. In particular, we saw that the longwave cooling from the dry subsiding region surrounding clouds is key. Most studies of deep convection focus on the moist region where clouds and convection occur. The discovery of self-aggregation thus highlighted the need to investigate the dry regions devoid of deep clouds as well. It could also help shed new light into challenging geophysical open questions, notably the Madden-Julian Oscillation (Kerry Emanuel and Marat Khairoutdinov, personal communication) and tropical cyclogenesis (Muller and Romps, 2018).

## 1.5 Response of the hydrological cycle to climate change

### 1.5.1 Context

In this section, we address the important question of the response of precipitation extremes to global warming. As in the previous section, we focus on tropical convection. Indeed, tropical precipitation extremes are particularly challenging for climate models. The “pop-corn” small-scale nature of convection there (compared the mid-latitudes where clouds and convection are embedded in large-scale low and high pressure frontal systems) implies that coarse-resolution global climate models have to rely on convective parameterizations to represent convective processes in the tropics.

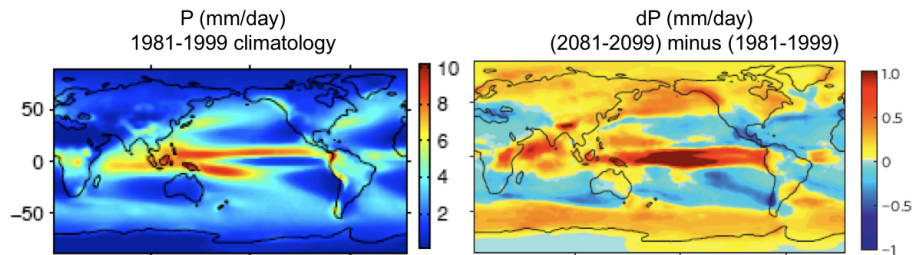


**Fig. 1.18** Mean precipitation climatology (left) and change in mean precipitation with global warming (right), illustrating the “rich-get-richer” pattern. High-precipitation regions (tropics and extratropics) have enhanced precipitation, and low-precipitation regions (subtropics) have decreased precipitation (after Muller and O’Gorman, 2011); © 2011, Springer Nature.

Despite uncertainties in those parameterizations, global climate models robustly predict a pattern of mean precipitation changes with warming now known as the “rich-get-richer” pattern. Rainy regions (tropics and extratropics figure 1.18) become rainier, and regions with little precipitation (subtropics figure 1.18) receive even less rain. This can be understood via simple thermodynamics (Held and Soden, 2006; Muller and O’Gorman, 2011). If changes in relative humidity are small, as is the case in climate models, we expect atmospheric water vapor to increase with warming following the Clausius-Clapeyron equation (§1.3.3, equation (1.12)). Furthermore, if the atmospheric circulation does not change significantly, to leading order we expect regions with moisture convergence (and thus precipitation) to have increased moisture convergence due to the increased moisture. Similarly, regions with moisture divergence



are expected to have stronger moisture divergence, and hence decreased precipitation. (Actually moisture divergence and convergence are linked to precipitation minus evaporation; but the changes in precipitation have considerably more structure than the changes in evaporation, so that the above results on patterns of precipitation changes hold. Note also that the large-scale tropical circulation does change, it weakens slightly, see (Held and Soden, 2006) for more details.)

The global mean precipitation does not follow the Clausius-Clapeyron increase, as it is constrained by global energetics. Atmospheric energy balance implies that the global mean precipitation must balance the global mean radiative cooling (neglecting changes in the Bowen ratio), which increases at a slower rate of about  $2\% \text{ K}^{-1}$  (Held and Soden, 2006).

These results for mean precipitation are extremely robust between climate models, and well understood. But large-scale constraints have little direct relevance to precipitation extremes in tropical storms, and there is a large uncertainty of precipitation extremes in climate models (figure 1.19, (Kharin, Zwiers, Zhang and Hegerl, 2007)). This uncertainty is largest in the tropics due to uncertainties in convective parameterizations. Since simulations of tropical precipitation extremes with current global climate models are unreliable, progress on the problem of changing tropical precipitation extremes must rely on either theory, observations, or simulations that resolve the convective-scale processes. Here we will use theory and cloud-resolving simulations to address this question, in disorganized “pop-corn” convection at first, and then assessing the impact of convective organization on the results.

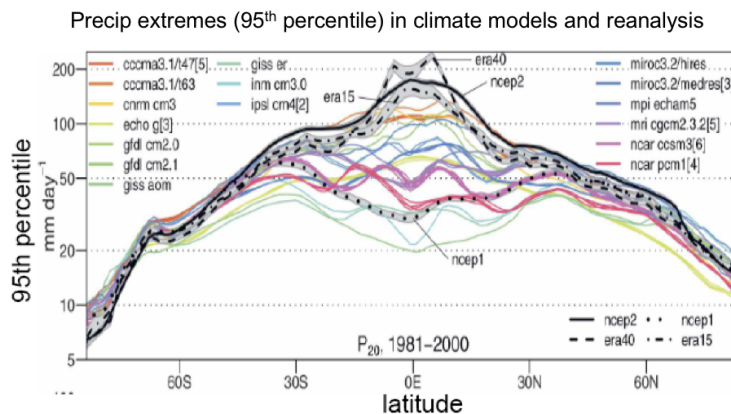


**Fig. 1.19** Precipitation extremes (95<sup>th</sup> percentile) in the different IPCC climate models (after Kharin et al., 2007). There is a large uncertainty in tropical precipitation extremes, due to uncertainties in convective parameterizations; © 2007 American Meteorological Society (AMS).

### 1.5.2 Amplification of precipitation extremes with warming: disorganized convection

What can we expect from theoretical considerations? If the dynamics do not change with warming, precipitation extremes can be expected to scale with the moisture convergence into deep convective updrafts, which would then scale with water vapor following the Clausius-Clapeyron equation. In the tropics, this equation predicts an increase of water vapor  $> 8\% \text{ K}^{-1}$  (O’Gorman and Muller, 2010). We will assess the accuracy of this thermodynamic expectation for precipitation extremes in cloud-resolving simulations, addressing the following questions:

- By how much do precipitation extremes increase with warming?
- How does it compare with the change in water vapor?
- How do vertical velocities in updrafts change, and how does it impact precipitation extremes?
- Can we derive a scaling that relates changes in precipitation extremes to mean quantities?

The cloud-resolving model used here is System for Atmospheric Modeling, or SAM, see §1.4.5 and (Khairoutdinov and Randall, 2003) for more details. Two simulations are performed, one with a sea-surface temperature of 300 K and another warmer simulation with a sea-surface temperature of 305 K. The radiative cooling profiles are imposed but are different for the two sea-surface temperatures, computed from short small-domain runs with the corresponding sea-surface temperatures (see (Muller, O’Gorman and Back, 2011) for more details). A weak background vertical shear is added, with horizontal wind decreasing from  $5 \text{ m s}^{-1}$  at low levels to zero at upper levels in the  $x$  direction. Note that this shear is too deep and too weak to generate a squall line, so that convection resembles somewhat randomly distributed pop-corn convection in these simulations.

Figure 1.20 shows composites around the location of extreme precipitation. We see that, as expected, precipitation is strongest in the dissipating stage of a cloud life cycle, as indicated by the downdrafts seen below the cloud (consistent with the schematic life cycle in figure 1.10). Also, as expected, there is preferred upward motion and cloud formation in the direction upshear (§1.4.2). The extremes, i.e. high percentiles, of daily precipitation are shown in the left panel of figure 1.21. We see that for a given percentile, the corresponding rainfall rate is always larger in the warmer simulation. Consistently, the ratio between the precipitation in the warm and in the cold runs is above 1. This ratio is shown in the middle panel for daily precipitation, and in the right panel for hourly precipitation. Although the values of precipitation extremes are sensitive to the temporal average, the *ratio* is not. In other words, the fractional increase in precipitation extremes is robust to the time scale used.

The fractional increase in precipitation extremes is found to asymptote at the highest percentiles, to  $\approx 7\% \text{ K}^{-1}$ . In order to clarify the physical origin of this value, we derive a scaling for extreme rainfall rates. From the equations of the model (Khairoutdinov and Randall, 2003), neglecting subgrid scale fluxes, and radiation which is expected to be a small contribution in locations of extreme precipitation (largely dominated by the latent heat term), (Muller, O’Gorman and Back, 2011) use the vertically-integrated

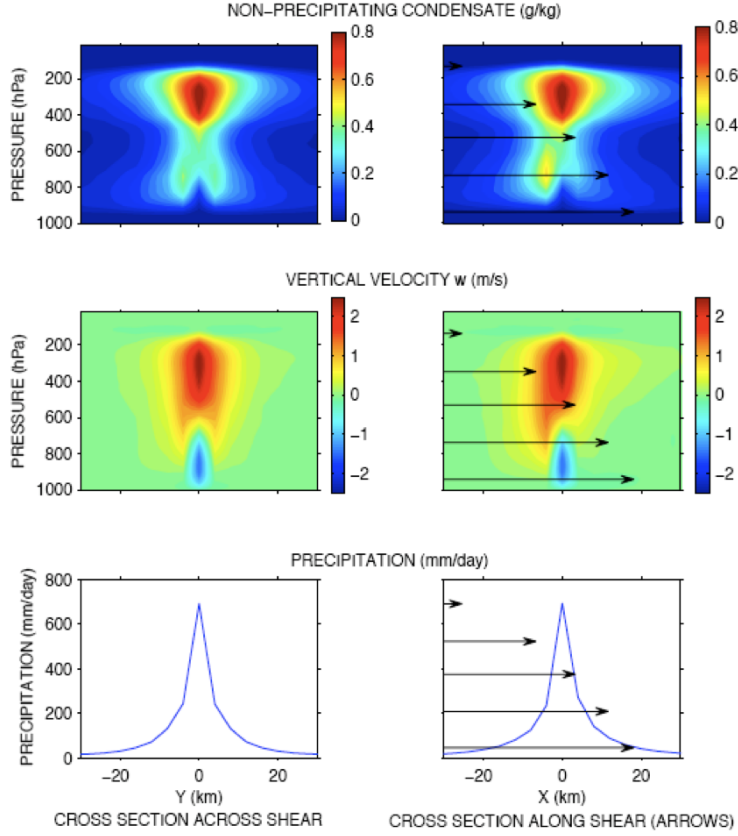


**Fig. 1.20** Composites in  $y$  (left) and  $x$  (right) directions around the location of extreme precipitation (placed at the origin). The top panels show non-precipitating condensates, the middle panels vertical velocity, and the bottom panels precipitation (after Muller et al., 2011); © 2011 American Meteorological Society (AMS).

dry static energy budget to derive the following scaling for extreme precipitation rates  $P_e$ :

$$P_e \approx \int w \frac{-\partial q_s}{\partial z} \bar{\rho} dz - \int \frac{D(L_v q_l + L_s q_i)}{L_v Dt} \bar{\rho} dz \quad (1.24)$$

$$\approx \epsilon_P \int w \frac{-\partial q_s}{\partial z} \bar{\rho} dz, \quad (1.25)$$

where  $\bar{\rho}$  denotes the reference density profile of the anelastic model SAM,  $q_s$  specific humidity at saturation,  $q_l$  liquid condensate amount,  $q_i$  solid condensate amount, and  $\epsilon_P$  the precipitation efficiency. Although this scaling was derived from the dry static energy equation, it resembles a water budget and can be interpreted as such: the first term on the right-hand side of equation (1.24) represents the total net condensation

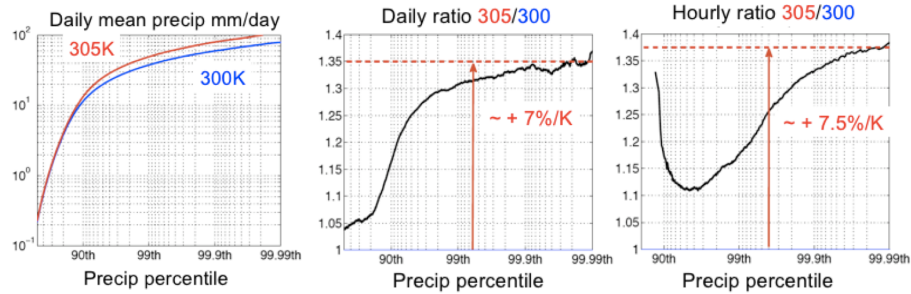


**Fig. 1.21** Values of daily precipitation extremes (i.e. high percentiles, left panel) in the cold (blue) and warm (red) simulations. The ratio between the warm and cold rainfall rates is shown in the middle panel. Similar results are obtained at hourly time scales (right panel, after Muller et al., 2011); © 2011 American Meteorological Society (AMS).

(and deposition) in the atmospheric column, including condensation from upward motion as well as evaporation of condensates maintaining a moist adiabatic lapse rate in downdraft regions. The second term on the right hand side accounts for an additional sink of water vapor, namely water vapor detrained as cloud condensates (liquid or ice). This sink can be included in a precipitation efficiency, where only a fraction of the net condensation precipitates out at the surface. In the limit  $\epsilon_P = 1$ , all the condensates precipitate out; in the limit  $\epsilon_P = 0$ , all condensates are advected from the column or build up in the column over the time scale in question.

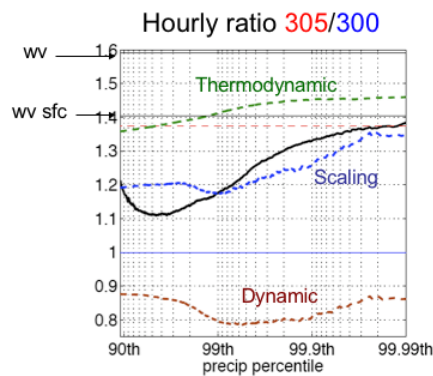


**Fig. 1.22** Increase in high percentiles of hourly mean precipitation (repeated from right panel of figure 1.21), and comparison with a theoretical scaling involving a dynamic and a thermodynamic contribution. The increase in atmospheric water vapor (wv) and low-tropospheric water vapor (wv sfc) are also shown (after Muller et al., 2011); © 2011 American Meteorological Society (AMS).

Assuming that changes in precipitation efficiency are small with warming, the change in precipitation can thus be decomposed into a dynamic and a thermodynamic contribution:

$$\delta P_e \approx \underbrace{\delta \left( \int -\frac{\partial q_s}{\partial z} w \bar{\rho} dz \right)}_{\text{scaling}} \approx \underbrace{\int \delta \left( -\frac{\partial q_s}{\partial z} \right) w \bar{\rho} dz}_{\text{thermodynamic}} + \underbrace{\int -\frac{\partial q_s}{\partial z} \delta (w \bar{\rho}) dz}_{\text{dynamic}}. \quad (1.26)$$

This simple scaling is found to be in very good agreement with numerical results (figure 1.22). Interestingly, the scaling predicts an increase in extreme precipitation which is smaller than the atmospheric water vapor increase, and closer to the increase in low-tropospheric moisture (figure 1.22). We will come back to this important result in the next section (see e.g. equation (1.29)). These results suggest that we can thus expect tropical precipitation extremes to increase following the low-level water vapor increase ( $< 6\% \text{ K}^{-1}$  in global climate models) instead of atmospheric humidity ( $> 8\% \text{ K}^{-1}$ , (O’Gorman and Muller, 2010)).

From figure 1.22, to first order, the amplification of precipitation extremes is well captured by the thermodynamic scaling. The dynamics play a secondary role, and tend to oppose the amplification of extreme rainfall rates with warming. We will come back to this point in the next section (see e.g. figure 1.25). We note also that these results seem to be robust to the model used, as similar increases in precipitation extremes, close to low-tropospheric moisture, have been found in another study using a different cloud-resolving model (Romps, 2011).

### 1.5.3 Impact of convective organization

As we saw in §1.4, convective organization is ubiquitous in the tropics, and is associated with extreme weather and strong rainfall rates. A key question is thus to determine how precipitation extremes in organized convection can be expected to change with warming. In this section, we assess the impact of organization on the results of the previous section, addressing the following questions:

- How do precipitation extremes in organized systems respond to warming?
- How sensitive is the amplification of precipitation extremes to the degree of organization?

To that end, we use vertical wind shear to organize the convection into squall lines, using the three simulations illustrated in figure 1.12: no shear, critical shear, and supercritical shear. We perform simulations at a control sea-surface temperature value of 300 K, and a warmer simulation at 302 K (see (Muller, 2013) for details). Figure 1.23 shows the high percentiles of precipitation in the various simulations, at cold and warm temperatures. As before, precipitation extremes are found to increase with warming, by about  $6\text{-}7\% \text{ K}^{-1}$ . We also see that for a given temperature, precipitation extremes are sensitive to vertical shear and almost double in the presence of shear, but increasing the shear from critical to supercritical shear has very little effect on the rainfall rates. This may not be too surprising since in the supercritical case the squall lines orient themselves so that the line-perpendicular component of the shear is critical. Therefore, one would expect rainfall rates similar to the ones obtained with critical shear as long as the shear is above critical.

What is perhaps more surprising is that despite very different organization, the amplification of precipitation extremes with warming is similar for all shears, though

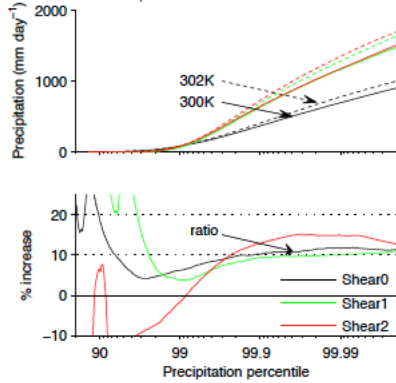


**Fig. 1.23** Increase in high percentiles of precipitation, in simulations with different shear strengths (after Muller, 2013); © 2013 American Meteorological Society (AMS).

it is slightly larger in the supercritical shear simulation. This behaviour is again well captured by the scaling in equation (1.26) (figure 1.24). As before, to leading order, the increase in precipitation extremes is determined by the thermodynamic contribution, and dynamics play a secondary role. But interestingly, the dynamic contribution is not robust to the shear: no shear or critical shear yield a negative contribution, opposing the amplification of precipitation extremes with warming. But supercritical shear yields a positive dynamic contribution, which explains the slightly stronger increase of precipitation extremes in that case. As in the previous section, the amplification of precipitation extremes is found to be closer to low-tropospheric humidity increase than to atmospheric humidity increase (not shown). These results thus confirm the conclusions of the previous section, the only difference being the dynamic contribution which can become positive in the presence of strong shear.

The fact that precipitation extremes follow low-tropospheric humidity, and not atmospheric humidity, can be understood using a simplified scaling, if we assume that  $\rho w$  at 500 hPa is a representative value for  $\rho w$  in equation (1.26):

$$\delta P_e \approx \delta \left( \int -\frac{\partial q_s}{\partial z} w \bar{\rho} dz \right) \quad (1.27)$$

$$\approx \delta \left( (w \bar{\rho})_{500hPa} \int -\frac{\partial q_s}{\partial z} dz \right) \quad (1.28)$$

$$\approx \underbrace{\delta \left( (w \bar{\rho})_{500hPa} q_{s,BL} \right)}_{\text{simplified scaling}}, \quad (1.29)$$

where  $q_{s,BL}$  denotes the saturation specific humidity in the boundary layer. If changes in relative humidity are small, precipitation extremes are thus expected to follow low-tropospheric water vapor.

The dynamic contribution deserves further investigation, as it is the contribution which is sensitive to the shear and thus the organization. Figure 1.25 shows the vertical profiles of  $\rho w$  and of  $w$  in the various simulations. We see that the decrease in vertical

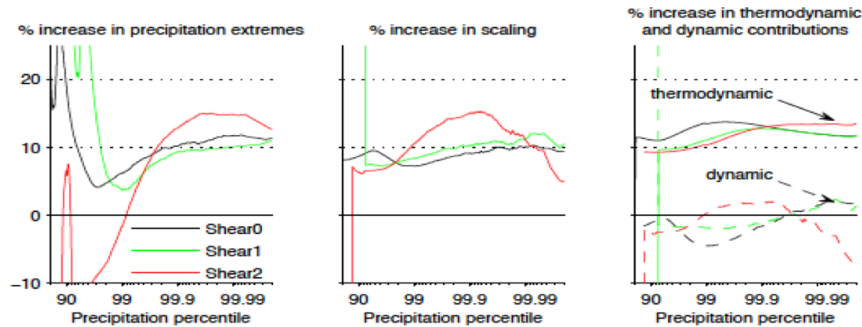


**Fig. 1.24** Increase in high percentiles of precipitation, and comparison with the theoretical scaling involving a dynamic and a thermodynamic contribution, in simulations with different shear strengths (after Muller, 2013); © 2013 American Meteorological Society (AMS).

mass fluxes with warming at critical and zero shear, is not observed with supercritical shear. Figure 1.25 also shows that the decrease in convective mass flux occurs despite an increase in the maximum updraft velocity (bottom panels). The former is more relevant to precipitation extremes.

#### 1.5.4 Discussion

Cloud-resolving simulations show that precipitation extremes increase with warming at a rate of about  $6\text{--}7\% \text{ K}^{-1}$  following the low-tropospheric humidity, yielding a smaller increase than atmospheric humidity. This behaviour can be understood using simple scalings, which relate precipitation extremes to thermodynamic and dynamic contributions. To leading order, precipitation extremes follow the thermodynamic scaling, even in the presence of convective organization. In fact, despite very different organizations, the amplification of precipitation extremes with warming is surprisingly robust in all the simulations shown on figure 1.12, closely following the increase in lower-tropospheric humidity.

Note that a large uncertainty regarding tropical precipitation extremes and their response to warming, is related to convective organization and its response to warming. Indeed, here we investigated the increase of precipitation extremes with warming *for a given degree of organization*. But figure 1.23 implies that a change in the degree of organization can lead to up to a doubling of extreme rainfall rates, while, for a given degree of organization precipitation extremes increase at about  $7\% \text{ K}^{-1}$  of warming. Thus the increase of precipitation extremes from a change in convective organization is larger than that associated with warming.

A recent observational study (Tan, Jakob, Rossow and Tselioudis, 2015) finds that recent trends in tropical precipitation can be linked to changes in the frequency of occurrence of organized mesoscale cloud systems. Improved fundamental understanding of convective organization and its sensitivity to warming is hence an area of priority for climate model development to achieve accurate rainfall projections in a warming climate.

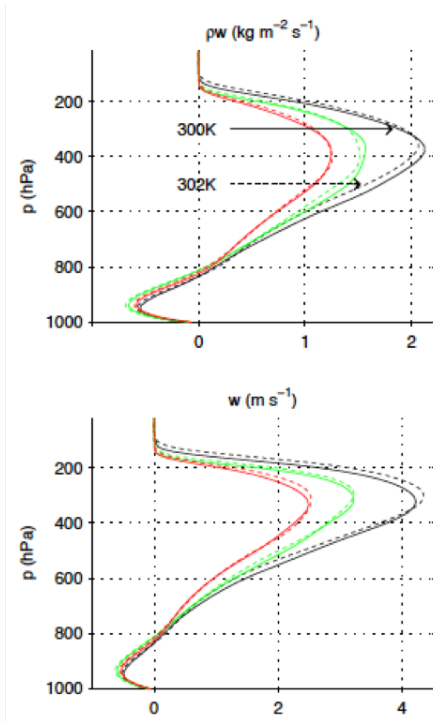


**Fig. 1.25** Change in vertical velocity and vertical mass flux with warming for the different shears. Despite an increase in vertical velocity, the mass flux decreases with warming (except for the supercritical shear in red). The latter is more relevant to precipitation extremes, explaining the negative dynamic contribution except with the strongest shear (figure 1.24, after Muller, 2013); © 2013 American Meteorological Society (AMS).

## 1.6 Clouds in a changing climate

### 1.6.1 Climate sensitivity

Climate sensitivity refers to the temperature change at equilibrium in response to a doubling of  $CO_2$ . In 1979, Charney published an early assessment of the impact of carbon dioxide on long-term climate, known as the “Charney Report” (Charney and Coauthors, 1979). In his report, Charney concluded that climate sensitivity ranged from 1.5 to 4.5 K, with a likely value of 3 K. He added that the key uncertainties in these estimates came from cloud feedbacks, the role of the ocean in carbon and heat uptake, and the prediction of regional precipitation changes. Since Charney’s report, several state-of-the-art IPCC reports have been published, summarizing the scientific knowledge on climate change, with increasing theoretical understanding and improved numerical tools. Despite almost 40 years of research in climate science, his aforementioned results remain largely true. Given the strong radiative impact of clouds, more work is desirable to reduce the large uncertainty in climate sensitivity associated with clouds and their response to climate change.



### 1.6.2 Clouds and radiation

In this section, we discuss the impact of clouds on the earth energy budget, i.e. on the top-of-atmosphere incoming radiation. The radiative impact of a cloud depends on its height and thickness. Low thick clouds have a high albedo, i.e. they reflect a significant amount of sunlight (figure 1.26a). But their temperature is close to the surface temperature, thus their thermal emission is close to the surface emission. So low clouds have little longwave (LW) effect, but are associated with strong shortwave (SW) cooling.

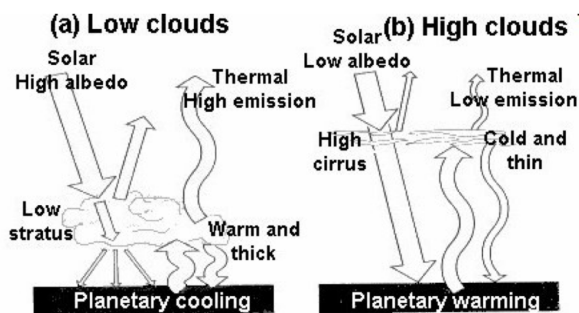


**Fig. 1.26** Schematic of the top-of-atmosphere radiative impact of low clouds (left) and high clouds (right). Figure from Turco 1997 ©2002 Oxford University Press, Inc.

High thin clouds on the other hand, are nearly transparent to the incoming solar shortwave radiation, with thus a low albedo (figure 1.26b). But their emission temperature is much lower than the surface temperature, implying a strong longwave signature. High clouds emit less to space due to their cold temperatures. So high clouds have little shortwave effect, but are associated with strong longwave warming.

Note that deep clouds (cumulonimbus) have both a strong albedo and a cold top emission temperature, so that the shortwave cooling is largely balanced by the longwave warming. Their radiative impact at the top of the atmosphere is nearly neutral.

Quantitatively, the *cloud radiative effect* is a measure of the cloud impact on the earth energy budget (i.e. incoming radiation at the top of the atmosphere). It is defined as the difference between the all-sky and the clear-sky flux (defined positive for warming):

- shortwave radiative effect =  $SW_{\text{in all sky}} - SW_{\text{in clear sky}}$  (typically  $< 0$  because of low clouds cooling)
- longwave radiative effect =  $LW_{\text{in all sky}} - LW_{\text{in clear sky}}$  (typically  $> 0$  because of high clouds warming)

The annual mean globally averaged LW cloud radiative effect is about  $+30 \text{ W m}^{-2}$ , and the SW cloud radiative effect  $-50 \text{ W m}^{-2}$ . In the net, the annual mean cloud radiative effect is thus negative and  $\approx -20 \text{ W m}^{-2}$ . This value can be compared to the radiative forcing associated with a doubling of  $CO_2$   $+4 \text{ W m}^{-2}$ . Clarifying how clouds respond to climate change is thus crucial to accurately estimate climate

sensitivity.

The *cloud radiative forcing* quantifies the difference between all-sky and clear-sky flux changes, providing a measure of the contribution of clouds to climate sensitivity. The net cloud radiative forcing is the sum of the longwave and the shortwave forcings, by convention  $< 0$  if clouds oppose warming, and  $> 0$  if clouds strengthen warming. Key questions are thus:

- How will clouds respond to increased  $CO_2$ ?
- Can we formalize the link between clouds and climate sensitivity?

The latter question will be addressed first, in the next section, where we introduce a classical framework widely used to quantify climate feedbacks and their contribution to climate sensitivity. The former question is still an active area of research, and the following section will present a brief overview of the physical processes believed to contribute significantly to the cloud feedback and its spread in climate models.

### 1.6.3 Quantifying climate feedbacks

As discussed in §1.4.5 (see e.g. equation (1.18)), the net incoming radiation at the top of the atmosphere is proportional to

$$R = \frac{S_0(1 - a)}{4} - OLR,$$

where  $OLR$  denotes the outgoing longwave radiation  $\sigma T_e^4$ . There is equilibrium when  $R = 0$ . Now let's imagine a forcing, such that  $\Delta R > 0$ . The dependence of  $OLR$  on temperature constitutes the main restoring force towards Earth's energy balance. Thus temperatures need to warm to reach the new equilibrium such that  $\Delta R = 0$ . It has been found from model experiments that to leading order, the radiative response can be assumed proportional to the global average surface air temperature change.

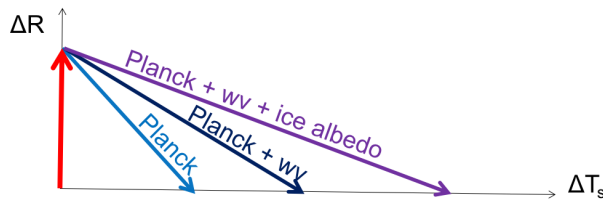


**Fig. 1.27** Global mean surface temperature response  $\Delta T_s$  to a radiative forcing  $\Delta R$  due to the Planck response (light blue), including as well the water vapor feedback (dark blue), and including the ice albedo feedback (purple). Each additional positive feedback implies that the surface temperature needs to increase more in order to reach equilibrium  $\Delta R = 0$ .

We can suppose that

$$OLR = f(CO_2, wv, cld)\sigma T_s^4,$$

where  $T_s$  denotes surface temperature,  $wv$  water vapor and  $cld$  cloud. If  $CO_2$  abruptly increases, the emission level goes up, thus the emission temperature goes down and

$OLR$  is smaller, so that  $\Delta R = F > 0$  (red arrow figure 1.27). If only  $T_s$  responds to the perturbation, a positive  $\Delta T_s > 0$  is needed to reach a new equilibrium  $\Delta R = 0$  (Planck response on figure 1.27).

Now if water vapor also increases as  $T_s$  increases, as can be expected from the Clausius-Clapeyron equation (1.12), the greenhouse effect of water vapor implies that a larger  $\Delta T_s$  is needed to reach equilibrium (Planck+wv on figure 1.27). If additionally the ice cover decreases with warming, the associated albedo decrease implies than an even larger  $\Delta T_s$  is needed (Planck+wv+ice albedo on figure 1.27).

These physical considerations can be formalized by assuming  $R = R(CO_2, T_s)$  and writing the radiative imbalance as

$$\Delta R = \left( \frac{\partial R}{\partial CO_2} \right)_{T_s} \Delta CO_2 + \left( \frac{\partial R}{\partial T_s} \right)_{CO_2} \Delta T_s \quad (1.30)$$

$$\Leftrightarrow \Delta R = F + \lambda \Delta T_s, \quad (1.31)$$

where  $F$  is the instantaneous radiative forcing due to increased  $CO_2$  (in  $W\ m^{-2}$ ), and  $\lambda = (\partial R / \partial T_s)_{CO_2}$  is the so-called feedback parameter (in  $W\ m^{-2}\ K^{-1}$ ). If  $\lambda < 0$ , the feedback is stabilizing, if  $\lambda > 0$ , the feedback is destabilizing the warming.

Note that  $\Delta R = 0$  yields

$$\Delta T_{eq} = -\frac{F}{\lambda}. \quad (1.32)$$

For a doubling of  $CO_2$ , this is the equilibrium climate sensitivity. Figures such as figure 1.27 are known as Gregory plots (Gregory, Ingram, Palmer, Jones, Stott, Thorpe, Lowe, Johns and Williams, 2004). Its application to a  $4 \times CO_2$  simulation is shown in figure 1.28 (Gregory, Ingram, Palmer, Jones, Stott, Thorpe, Lowe, Johns and Williams, 2004). The increased  $4 \times CO_2$  yields a positive anomalous net incoming radiative flux, which decreases in time as the surface air temperature increases, until a new equilibrium  $\Delta R = 0$  is reached. The slope of the line is the feedback parameter  $\lambda$ .

We can extend the above analysis to include the contribution of the various feedbacks to the feedback parameter:

$$\frac{\partial R}{\partial T_s} = \sum_x \frac{\partial R}{\partial x} \frac{\partial x}{\partial T_s} \Leftrightarrow \lambda = \lambda_{Planck} + \underbrace{\lambda_{wv} + \lambda_{ice} + \lambda_{cld} + \dots}_{\text{influence of each feedback } x \text{ on climate sensitivity}} \quad (1.33)$$

This framework helps interpret inter-model differences in climate sensitivity (figure 1.29, (Dufresne and Bony, 2008)). Based on global climate model simulations, clouds are found to be the largest source of uncertainty between models. Explaining this spread remains an active area of research, and various physical processes involved are discussed in the next section. For more information on how to compute those feedback parameters, notably on the Kernel approach, the interested reader is referred to (Soden, Held, Colman, Shell, Kiehl and Shields, 2008).

#### 1.6.4 Cloud feedback processes

How do different cloud types contribute to global cloud feedbacks? Figure 1.30 shows the cloud feedbacks in several climate models (from (Zelinka, Klein, Taylor, Andrews,

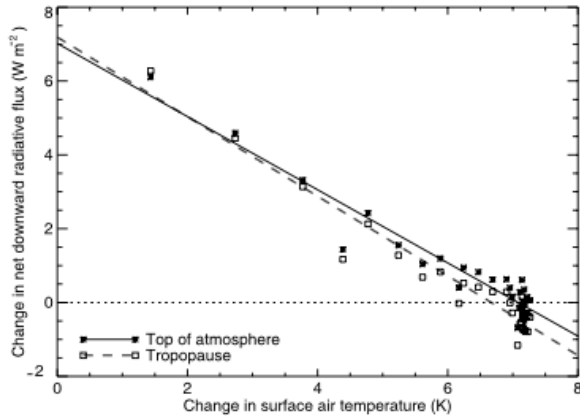


**Fig. 1.28** Gregory plot showing the time evolution of net downward radiative imbalance at the top of atmosphere (and tropopause) in response to a quadrupling of  $CO_2$  in a climate model (HadSM3), as a function of surface air temperature anomaly (1.5 m height). The dotted line represents radiative equilibrium  $\Delta R = 0$  (from Gregory et al., 2004); © 2004, John Wiley and Sons.

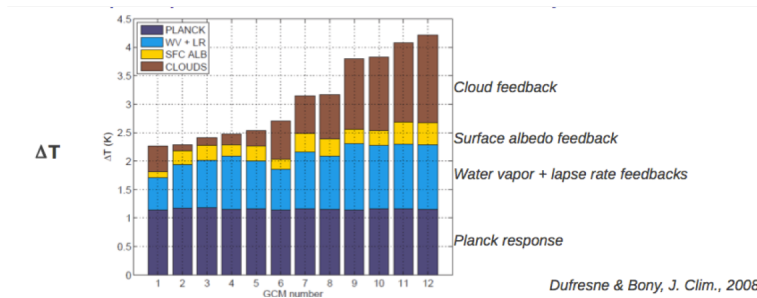


**Fig. 1.29** Contributions of various feedbacks to equilibrium climate sensitivity in global climate models (GCMs) (from Dufresnes and Bony, 2008). The cloud feedback is responsible for the largest spread between models; © 2008 American Meteorological Society (AMS).

Webb, Gregory and Forster, 2013)). The spread between models largely comes from low clouds. Note that high clouds have a large spread in longwave and shortwave separately, but these tend to cancel, since as mentioned above high deep clouds have both a strong albedo and a cold top emission temperature. So the shortwave cooling is largely balanced by the longwave warming.

Alternatively, we can split the cloud feedback into cloud amount, altitude and optical depth (figure 1.30 right). The latter yields a negative cloud feedback, associated with increased cloud optical depth. This negative cloud optical depth feedback arises mostly from the extratropics, with a robust increase in cloud optical depth at latitudes poleward of about  $40^\circ$ . This high-latitude cloud optical thickness response is likely related to changes in the phase and/or total water content of clouds (Zelinka, Klein,

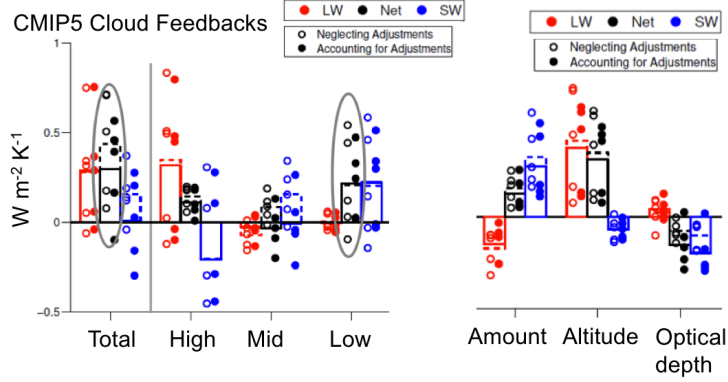


**Fig. 1.30** Total cloud feedback in several CMIP5 models (left), contributions from high, middle and low clouds (middle), and contributions split into amount, altitude and optical depth (right) (adapted from Zelinka et al., 2013; the interested reader is also referred to Zelinka et al., 2016 for a larger ensemble of models). The low-cloud feedback dominates the spread between models. © 2013 American Meteorological Society (AMS).

Taylor, Andrews, Webb, Gregory and Forster, 2013).

Cloud altitudes yield a positive cloud feedback contribution, associated with higher clouds. In a warmer climate, climate models robustly predict a rise in upper-level clouds. So do cloud-resolving models. A theoretical explanation for this behavior was proposed by (Hartmann and Larson, 2002), using the radiative-convective equilibrium framework (§1.4.5). It is known as the FAT hypothesis, or fixed anvil temperature hypothesis. This hypothesis implies that tropical anvil clouds detrain at a fixed temperature independent of surface warming. This behaviour is closely related to the shape of the radiative cooling profile.

More precisely, in radiative-convective equilibrium, the depth of the convection layer is determined by the depth of the atmospheric layer destabilized by radiation (figure 1.31). In clear skies, the radiative cooling is balanced by adiabatic heating through subsidence

$$\omega = \frac{Q}{\sigma},$$

where  $\omega$  denotes vertical velocity,  $Q$  radiative cooling, and  $\sigma$  static stability. The strong decline of radiative cooling with altitude around 200 hPa (figure 1.31) must thus be accompanied by a strong horizontal convergence of mass in clear skies at that level

$$-\nabla \cdot V = \frac{\partial \omega}{\partial p}.$$

This convergence in subsidence regions must in turn be balanced by a strong divergence of mass from the convective regions. The divergence of mass is associated with the frequent occurrence of convective anvil clouds at this level.

The height of anvils is thus closely related to the region of strong decline of radiative cooling. Water vapor is responsible for most of the cooling of the tropical upper

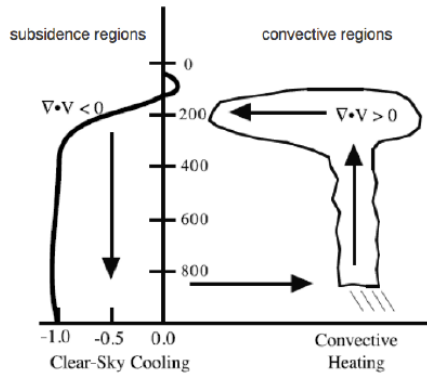


**Fig. 1.31** Two box schematic representation of convection, with radiative cooling in clear sky subsidence regions balanced by convective heating in convective regions (from Hartmann and Larson, 2002); © 2002, John Wiley and Sons..

troposphere. The height at which the cooling has a strong vertical gradient is thus determined by the amount of water above it. Since the saturation vapor pressure is a function of temperature only (equation (1.12)), if the relative humidity is fixed, the profile of water vapor pressure in the vertical is determined by the temperature, and the temperature at which this gradient occurs will be roughly constant, including in climate change scenarios. The implication of the FAT hypothesis for climate is that cloud tops do not warm in step with surface and atmospheric temperatures. In other words, the tropics become less efficient at radiating away heat, yielding a positive longwave cloud feedback.

Finally, cloud amounts yield a positive feedback, associated with decreased cloud fraction. In many regions, the feedback from cloud amounts is not robust between models, particularly in the tropics. Several mechanisms have been proposed for the decreased low cloud amount, including the role of enhanced surface fluxes deepening the boundary layer, and hence the mixing of dry and warm air to the surface, leading to decreased cloudiness as climate warms (Rieck, Nuijens and Stevens, 2012). Radiative effects of clouds have also been suggested to be important. Low-level clouds contribute to their own maintenance through their radiative effect, which could explain the large spread of low cloud feedbacks (Brient and Bony, 2012).

For deep clouds, the FAT theory does not predict the change in cloud amount. How the deep cloud cover will change with warming remains an open question. Notably, convective organization can impact cloud cover, and as we saw in §1.4 convective organization is still an active area of research. More work is desirable to clarify the response of convective organization and cloud cover, both low and high clouds, to warming, as well as implications for the hydrological cycle, including mean and extreme precipitation.

# References

- Bohren, C F and Albrecht, B A (2000). Atmospheric thermodynamics.
- Bony, S, Stevens, B, Frierson, D, Jakob, C, Kageyama, M, Pincus, R, Shepherd, T G, Sherwood, S C, Siebesma, A P, Sobel, A H et al. (2015). Clouds, circulation and climate sensitivity. *Nature Geoscience*, **8**(4), 261.
- Bretherton, C S, Blossey, P N, and Khairoutdinov, M (2005). An energy-balance analysis of deep convective self-aggregation above uniform sst. *Journal of the atmospheric sciences*, **62**(12), 4273–4292.
- Brient, F and Bony, S (2012). How may low-cloud radiative properties simulated in the current climate influence low-cloud feedbacks under global warming? *Geophysical Research Letters*, **39**(20).
- Charney, J G and Coauthors (1979). *Carbon dioxide and climate: a scientific assessment*. National Academy of Science, Washington, DC.
- COMET program (2007-2018). MetEd. Website of the University Corporation for Atmospheric Research (UCAR). <https://www.meted.ucar.edu/index.php>.
- Dufresne, J-L and Bony, S (2008). An assessment of the primary sources of spread of global warming estimates from coupled atmosphere–ocean models. *Journal of Climate*, **21**(19), 5135–5144.
- Emanuel, K A (1986). An air-sea interaction theory for tropical cyclones. part i: Steady-state maintenance. *Journal of the Atmospheric Sciences*, **43**(6), 585–605.
- Emanuel, K A (1994). *Atmospheric convection*. Oxford University Press on Demand.
- EUMETSAT (2017). Year of Weather. Website. <https://www.youtube.com/watch?v=9YAXEHLNphY>.
- Garner, S T and Thorpe, A J (1992). The development of organized convection in a simplified squall-line model. *Quarterly Journal of the Royal Meteorological Society*, **118**(503), 101–124.
- Gregory, J M, Ingram, W J, Palmer, M A, Jones, G S, Stott, P A, Thorpe, R B, Lowe, J A, Johns, T C, and Williams, K D (2004). A new method for diagnosing radiative forcing and climate sensitivity. *Geophysical Research Letters*, **31**(3).
- Hartmann, D L and Larson, K (2002). An important constraint on tropical cloud-climate feedback. *Geophysical Research Letters*, **29**(20), 12–1.
- Held, I M and Soden, B J (2006). Robust responses of the hydrological cycle to global warming. *Journal of climate*, **19**(21), 5686–5699.
- Houze Jr, R A (2014). *Cloud dynamics*. Volume 104. Academic press.
- ISCCP (2009). International Satellite Cloud Climatology Project. Website. <https://isccp.giss.nasa.gov/climanal2.html>.
- Khairoutdinov, M F and Randall, D A (2003). Cloud resolving modeling of the arm summer 1997 iop: Model formulation, results, uncertainties, and sensitivities. *Journal of the Atmospheric Sciences*, **60**(4), 607–625.

- Kharin, V V, Zwiers, F W, Zhang, X, and Hegerl, G C (2007). Changes in temperature and precipitation extremes in the ipcc ensemble of global coupled model simulations. *Journal of Climate*, **20**(8), 1419–1444.
- Kiladis, G N, Wheeler, M C, Haertel, P T, Straub, K H, and Roundy, P E (2009). Convectively coupled equatorial waves. *Reviews of Geophysics*, **47**(2).
- Manabe, S and Strickler, R F (1964). Thermal equilibrium of the atmosphere with a convective adjustment. *Journal of the Atmospheric Sciences*, **21**(4), 361–385.
- Mapes, B E (1993). Gregarious tropical convection. *Journal of the atmospheric sciences*, **50**(13), 2026–2037.
- Matsuno, T (1966). Quasi-geostrophic motions in the equatorial area. *Journal of the Meteorological Society of Japan. Ser. II*, **44**(1), 25–43.
- Muller, C J (2013). Impact of convective organization on the response of tropical precipitation extremes to warming. *Journal of Climate*, **26**(14), 5028–5043.
- Muller, C J and Bony, S (2015). What favors convective aggregation and why? *Geophysical Research Letters*, **42**(13), 5626–5634.
- Muller, C J and Held, I M (2012). Detailed investigation of the self-aggregation of convection in cloud-resolving simulations. *Journal of the Atmospheric Sciences*, **69**(8), 2551–2565.
- Muller, C J and O’Gorman, P A (2011). An energetic perspective on the regional response of precipitation to climate change. *Nature Climate Change*, **1**(5), 266.
- Muller, C J, O’Gorman, P A, and Back, L E (2011). Intensification of precipitation extremes with warming in a cloud-resolving model. *Journal of Climate*, **24**(11), 2784–2800.
- Muller, C J and Romps, D M (2018). Acceleration of tropical cyclogenesis by self-aggregation feedbacks. *Proceedings of the National Academy of Sciences*, 201719967.
- O’Gorman, P A and Muller, C J (2010). How closely do changes in surface and column water vapor follow clausius–clapeyron scaling in climate change simulations? *Environmental Research Letters*, **5**(2), 025207.
- Rieck, M, Nuijens, L, and Stevens, B (2012). Marine boundary layer cloud feedbacks in a constant relative humidity atmosphere. *Journal of the Atmospheric Sciences*, **69**(8), 2538–2550.
- Romps, D M (2011). Response of tropical precipitation to global warming. *Journal of the Atmospheric Sciences*, **68**(1), 123–138.
- Rossow, W B and Schiffer, R A (1999). Advances in understanding clouds from isccp. , **80**(11), 2261–2288.
- Rotunno, R, Klemp, J B, and Weisman, M L (1988). A theory for strong, long-lived squall lines. *Journal of the Atmospheric Sciences*, **45**(3), 463–485.
- Soden, B J, Held, I M, Colman, R, Shell, K M, Kiehl, J T, and Shields, C A (2008). Quantifying climate feedbacks using radiative kernels. *Journal of Climate*, **21**(14), 3504–3520.
- SSEC (2018). Space Science and Engineering Center. Website. <https://www.ssec.wisc.edu/data/geo-list/>.
- Stevens, B (2005). Atmospheric moist convection. *Annu. Rev. Earth Planet. Sci.*, **33**, 605–643.
- Tan, J, Jakob, C, Rossow, W B, and Tselioudis, G (2015). Increases in tropical rainfall



48 *References*

- driven by changes in frequency of organized deep convection. *Nature*, **519**(7544), 451.
- Wheeler, M and Kiladis, G N (1999). Convectively coupled equatorial waves: Analysis of clouds and temperature in the wavenumber–frequency domain. *Journal of the Atmospheric Sciences*, **56**(3), 374–399.
- Wing, A A, Emanuel, K, Holloway, C E, and Muller, C (2017). Convective self-aggregation in numerical simulations: a review. *Surveys of Geophysics*, 1–25.
- Zelinka, M D, Klein, S A, Taylor, K E, Andrews, T, Webb, M J, Gregory, J M, and Forster, P M (2013). Contributions of different cloud types to feedbacks and rapid adjustments in cmip5. *Journal of Climate*, **26**(14), 5007–5027.